Metabolomic profiling of rare cell populations isolated by flow cytometry from tissues

Andrew W. DeVilbiss[1], Zhiyu Zhao[1], Misty S. Martin-Sandoval[1], Jessalyn M. Ubellacker[1], Alpaslan Tasdogan[1], Michalis Agathocleous[1], Thomas P. Mathews[1,2]*, Sean J. Morrison[1,2]*

[1]Children's Research Institute and Department of Pediatrics, University of Texas Southwestern Medical Center, Dallas, Texas 75390, USA

[2]Howard Hughes Medical Institute, University of Texas Southwestern Medical Center, Dallas, Texas 75390, USA

*Co-corresponding authors: Thomas.Mathews@UTSouthwestern.edu; Sean.Morrison@UTSouthwestern.edu

Impact statement: A method was developed for the metabolomic analysis of small numbers of flow cytometrically isolated cells from rare cell populations such as hematopoietic stem cells and circulating cancer cells.

Little is known about the metabolic regulation of rare cell populations because most metabolites are hard to detect in small numbers of cells. We previously described a method for metabolomic profiling of flow cytometrically-isolated hematopoietic stem cells (HSCs) that detects 60 metabolites in 10,000 cells (Agathocleous et al., 2017). Here we describe a new method involving hydrophilic liquid interaction chromatography and high-sensitivity orbitrap mass spectrometry that detected 160 metabolites in 10,000 HSCs, including many more glycolytic and lipid intermediates. We improved chromatographic separation, increased mass resolution, minimized ion suppression, and eliminated sample drying. Most metabolite levels did not significantly change during cell isolation. Mouse HSCs exhibited increased glycerophospholipids relative to bone marrow cells and methotrexate treatment altered purine biosynthesis. Circulating human melanoma cells were depleted for purine intermediates relative to subcutaneous tumors, suggesting decreased purine synthesis during metastasis. These methods facilitate the routine metabolomic analysis of rare cells from tissues.

Introduction

Metabolomics is typically performed using millions of cells, often using cultured cells, whole tissues, or tumor specimens (Jang et al., 2018). This measures average metabolite levels across the cells in a specimen but is blind to metabolic differences among cells in the same sample. As a result, we have limited insight into metabolic heterogeneity among cells within tissues or tumors (Kim and DeBerardinis, 2019, Muir et al., 2018). This limitation is particularly apparent when considering rare cells, such as stem cells or circulating cancer cells, that may be metabolically different from other cells. The difficulty of performing metabolomics on small numbers of these cells is compounded by the need to purify them from tissues, introducing additional technical challenges for metabolic analysis (Binek et al., 2019, Llufrio et al., 2018, Lau et al., 2020).

It is extremely difficult to isolate a million cells from a rare cell population by flow cytometry. One study isolated over 1 million $CD34^{-}Flt3^{-}Lineage^{-}Sca\text{-}1^{+}c\text{-}kit^{+}$ hematopoietic stem cells (HSCs) by flow cytometry but pooled bone marrow cells from 120 mice to do it, precluding the analysis of multiple replicates or routine application of this approach (Takubo et al., 2013). Metabolomics has also been performed on hundreds of thousands of flow cytometrically-isolated $Lineage^{-}Sca\text{-}1^{+}c\text{-}kit^{+}$ (LSK) cells (Naka et al., 2015, Karigane et al., 2016), a more heterogeneous population of hematopoietic stem and progenitor cells. Since only a small minority of these cells are HSCs, this strategy provides limited insight into metabolite levels in HSCs themselves. Others have characterized the phenotypes of mutant mice or metabolism in cultured hematopoietic stem and progenitor cells (Simsek et al., 2010, Ito et al., 2012, Ito et al., 2016, Ito et al., 2019, Wang et al., 2014, Ansó et al., 2017). However, it remains difficult to routinely compare metabolite levels between HSCs and other hematopoietic progenitors.

Metabolites have been profiled in single cells (Evers et al., 2019, Comi et al., 2017). However, these studies often use very large cells like Xenopus eggs (Onjiko et al., 2015) or Aplysia neurons (Nemes et al., 2012). Other single cell analyses have focused on small numbers of metabolites or specific subsets of metabolites (Luo and Li, 2017). Single cell metabolomics methods often involve mass spectrometry without chromatographic separation, making it more difficult to identify the detected species (Duncan et al., 2019, Ali et al., 2019).

We recently described a method for metabolomic analysis of highly purified, flow cytometrically isolated $CD150^{+}CD48^{-}$LSK HSCs that detected approximately 60 metabolites in 10,000 cells (Agathocleous et al., 2017). Cells were kept cold during the entire purification process and sorted directly into 80% methanol to immediately quench enzymatic activity and extract metabolites. This method revealed that HSCs take up more ascorbate than other hematopoietic cells and depend upon ascorbate for epigenetic regulation and leukemia suppression, though coverage of many metabolic pathways was limited.

The challenge of performing metabolomic analysis in rare cells is not limited to stem cells as illustrated by a paucity of information about the metabolic state of circulating cancer cells. Many tumors spontaneously shed cancer cells into the blood (Micalizzi et al., 2017) but these cells are extremely rare, limiting the amount of material for analysis. We have developed methods for the flow cytometric isolation and characterization of circulating human melanoma cells from the blood of xenografted mice (Piskounova et al., 2015, Tasdogan et al., 2020). These cells undergo reversible metabolic changes during metastasis to survive oxidative stress, but these changes are just beginning to be characterized. Mass spectrometric analysis of single circulating cancer cells from the blood of patients revealed metabolites that differed among various kinds of cancer cells (Hiyama et al., 2015, Abouleila et al., 2019). Fluorescent probes have also been used to characterize metabolism in circulating cancer cells (Li et al., 2019).

Here we present a new method for the metabolomic analysis of rare stem cell and cancer cell populations isolated by flow cytometry. We have increased the number of metabolites we can detect in 10,000 HSCs to approximately 160. Using this method, the levels of most metabolites did not significantly change during cell preparation and sorting.

RESULTS

Chromatography and mass spectrometry

In order to significantly increase the numbers of metabolites we detected in small numbers of flow cytometrically isolated cells, we re-examined the chromatography and mass spectrometry approaches we used. A key limitation is discriminating the low levels of metabolites present in small numbers of cells from background signals. Background reflects contamination from various sources as well as the co-association of salts with organic compounds in mass spectrometers to generate organic salt clusters (matrix ions) that obscure the detection of metabolites. We reasoned we could improve the signal to noise ratio in low

abundance samples and reduce interference by matrix ions by transitioning to a mass spectrometer with higher mass resolving power.

We chose a Q-Exactive HF-X hybrid quadrupole-orbitrap mass spectrometer (ThermoScientific) because it offers four advantages over the triple-quadrupole mass spectrometer used in our previous method (Agathocleous et al., 2017). First, whereas the triple-quadrupole instrument acquires data for a predetermined number of metabolites, the orbitrap instrument captures spectra for the full mass range (80 – 1200 Daltons) with each scan, greatly increasing the number of metabolites detected. Second, orbitrap mass analyzers have higher mass resolving power and higher mass accuracy, increasing the ability to discriminate relevant analytes from background ions. Third, through untargeted acquisition of product ion spectra, orbitrap instruments enable the comparison of spectra from experimental samples with annotated spectrum libraries for high-confidence identification of metabolites. Finally, compared to other orbitrap models, the HF-X front end optics increase the number of ions that can pass into the mass spectrometer, boosting the signal from low abundance analytes.

We also wondered if a hydrophilic interaction liquid chromatography (HILIC) system would improve the separation of polar metabolites as compared to the reverse phase chromatography method in our original study (Agathocleous et al., 2017). To test this, we extracted metabolites from $5x10^6$ mouse whole bone marrow (WBM) cells in 500 µl of 80% methanol, dried the extracts in a vacuum concentrator, and reconstituted in water for reverse phase chromatography or 80% methanol for HILIC. Polar analytes eluted from the reverse phase column between 3 and 5 minutes, and from the HILIC column between 2 and 15 minutes, indicating that HILIC improved polar metabolite separation (data not shown).

When we ran high abundance samples either by reverse phase or HILIC we identified hundreds of metabolites by spectral database matching and manual peak review (data not shown). However, the improved metabolite separation and peak quality we observed with HILIC yielded more high confidence identifications of metabolites via spectral database matching

alone (Figure 1A). HILIC also enabled the detection of early-eluting lipid metabolites, which were not detected using reverse phase chromatography. They were well-resolved chromatographically (Figure 1 – figure supplement 1 A-D) and were detected within the linear range of the mass spectrometer (Figure 1 – figure supplement 1 E-H). Finally, HILIC eliminated the requirement for sample drying, which can alter the levels of certain metabolites and increase contamination (Lu et al., 2017). We thus selected HILIC for further method development.

We also fundamentally changed our approach to data analysis. To determine which metabolites were detected in low abundance samples we created a list of metabolites with known masses and chromatographic retention times from the analysis of high abundance samples. We first used unbiased metabolite identification software (Compound Discoverer) to compare experimentally observed mass spectra with annotated spectrum libraries to identify 571 metabolites. We confirmed the identities of each metabolite in the library by reviewing the MS2 spectra for each metabolite. We confirmed the retention times and mass spectra for over 450 metabolites in the library by running chemical standards. This library was used to determine how many metabolites were detected in low abundance samples by manually analyzing chromatographic peaks derived from extracts of 100,000 WBM cells. This resulted in a low abundance library containing 283 detectable metabolites that was used for manual metabolite quantitation in low abundance samples. This manual approach was more time consuming but more accurate than relying upon automated peak-calling algorithms, which often failed to accurately integrate LC-MS peaks from low-abundance samples.

Reducing sources of contamination

Background signals arose from the staining medium in which we suspended the cells, the flow cytometer sheath fluid, the solvent we used to extract metabolites from the sorted cells, and the drying and reconstitution of samples prior to liquid chromatography/mass spectrometry (LC-MS) (Agathocleous et al., 2017). While these very low levels of background would be

negligible when analyzing high abundance samples, they did interfere with the ability to detect some metabolites in low abundance samples.

When performing reverse phase separation, metabolites were extracted using 80% methanol and then dried in a vacuum concentrator so they could be reconstituted in water for chromatography (Agathocleous et al., 2017). Transitioning to HILIC made it possible to directly inject organic solvents into the column, without drying and reconstituting in water. To test if contamination was reduced by not drying in a vacuum concentrator, we sorted droplets of sheath fluid with no cells in volumes equivalent to that required to sort 10,000 cells and processed the samples side-by-side in three ways. Some samples were dried in a standard vacuum concentrator, then reconstituted in 80% methanol and injected into the HILIC column. Some samples were dried in a new vacuum concentrator housed in a HEPA-filtered PCR hood to minimize contamination from the air, then reconstituted in 80% methanol and injected into the HILIC column. The remaining samples were sorted into 80% methanol and injected directly into the HILIC column without drying. The highest level of background contamination was in the samples dried in the standard vacuum concentrator (Figure 1B). The lowest background was in the samples injected into the column without drying, suggesting drying increased contamination.

To test if we could detect more metabolites above background in low abundance samples if we did not dry and reconstitute, we sorted samples of 10,000 WBM cells, along with sheath fluid negative controls, and processed the samples side-by-side either with drying in a standard vacuum concentrator, with drying in a new vacuum concentrator in a HEPA-filtered PCR hood, or without drying. We detected 98, 123, or 130 metabolites significantly above sheath fluid background (always fold change > 2 and FDR < 0.05) in the samples dried in a standard vacuum concentrator, a HEPA-filtered vacuum concentrator, or undried, respectively (Figure 1C). We thus detected more metabolites above background in low abundance samples if we avoided sample drying and incorporated this approach into the method.

Acetonitrile extraction

Metabolites are most commonly extracted from cells using miscible aqueous-organic solvents, with the elimination of proteins, non-soluble components, and cellular debris by centrifugation. Different metabolites require different solvents for extraction (Rabinowitz and Kimball, 2007a). To test different solvents, we extracted metabolites from 100,000 pipetted WBM cells using 80% methanol in water, 40:40:20 acetonitrile:methanol:water, or 80% acetonitrile in water. Using HILIC and orbitrap mass spectrometry we detected an average of 317 metabolites in samples extracted with 80% acetonitrile and 266 or 273 metabolites in samples extracted with 80% methanol or 40:40:20 methanol:acetonitrile:water, respectively (Figure 1D). While we observed considerable overlap in the metabolites detected using each solvent, 80% acetonitrile yielded a number of metabolites that were not detected using the other solvents (Figure 1E). We thus selected 80% acetonitrile for further method development.

Ion suppression and cell numbers

Ion suppression of metabolite signals can occur as a result of the salt in the phosphate buffered saline (PBS) sheath fluid used for flow cytometric sorting: 1 to 3 nl of sheath fluid is sorted along with each cell depending on whether a 70 µm or 100 µm nozzle is used. Flow cytometry sheath fluid must contain salt to electrostatically charge droplets for sorting; sorting more cells also sorts more salt. When using reverse phase chromatography, we reduced ion suppression by using 0.5x PBS sheath fluid and a 70 µm nozzle in 4-way purity sort mode to minimize droplet volume (Agathocleous et al., 2017). After changing to HILIC, we retested whether 0.5x PBS or the 70 µm nozzle affected the number of metabolites we detected from 10,000 WBM cells. Sorting with the 70 µm nozzle increased the number of metabolites we could detect above sheath fluid background as compared to the 100 µm nozzle, regardless of PBS concentration (Figure 1F). We found no significant difference in the number of metabolites detected above background using 0.5x (157±2) versus 1.0x (149±9) PBS (Figure 1F).

We found 18 metabolites that significantly differed among samples sorted with 0.5x versus 1x PBS sheath fluid (always fold change > 2 and FDR < 0.05; see the list of metabolites in Figure 1 – Source data 2, Supplementary Table 1). Pathway enrichment analysis did not identify any pathways that were significantly enriched among the changed metabolites. It is unlikely that these differences are a consequence of hypotonic shock because the laminar flow within the cytometer minimizes the mixing of the cell sample buffer (1x HBSS) and the sheath fluid. Cells pass through the flow cytometer in less than a second and are immediately lysed upon sorting into the extraction solvent. Differences between 0.5x and 1x PBS sheath fluid are more likely to reflect reduced ion suppression in samples sorted with 0.5x PBS and altered metabolite extraction efficiency. We selected 0.5x PBS as the sheath fluid for further method development as we tended to detect somewhat more metabolites and higher levels of some metabolites when using 0.5x PBS.

Next we tested if the number of metabolites we detected above background increased with increasing numbers of cells. We pipetted 10,000, 20,000, 30,000, 50,000 or 100,000 WBM cells (in equal volumes of HBSS buffer) directly into 80% acetonitrile and quantitated metabolites. The number of metabolites detected above sheath fluid background increased significantly with increasing numbers of cells, from 157 ± 4 metabolites in 10,000 cells to 222 ± 9 metabolites in 100,000 cells (Figure 1G). In the same experiment, we detected an average of 155 ± 2 metabolites from 10,000 flow cytometrically sorted WBM cells (Figure 1G). We thus detected similar numbers of metabolites in flow cytometrically sorted and unsorted samples.

Effect of flow cytometry on metabolite levels

To determine if metabolic differences between cells are preserved during cell sorting using the methods described above, we sorted or pipetted 10,000 HNT-34 AML cells or 10,000 DND-41 T-ALL cells into 80% acetonitrile. We detected 143 to 167 metabolites above background in each sample. Principal component analysis revealed differences between sorted

and pipetted AML cells (Figure 1H; see the list of metabolites in Figure 1 – Source data 3, Supplementary Table 2) whereas differences among sorted and pipetted ALL cells were subtle (Figure 1H; see the list of metabolites in Figure 1 – Source data 4, Supplementary Table 3). 43 metabolites significantly differed between sorted and pipetted AML cells while 19 metabolites differed between sorted and pipetted ALL cells (fold change > 2 and FDR < 0.05). Pathway enrichment analysis revealed that metabolites that differed between sorted and pipetted AML cells were significantly enriched in “cysteine and methionine metabolism”. No pathways were significantly enriched among metabolites that differed between sorted and pipetted ALL cells.

Irrespective of whether cells were sorted or pipetted, similar differences were observed between AML and ALL cells. Among sorted samples, 85 metabolites significantly differed between AML and ALL cells while among pipetted samples, 71 of the same metabolites differed (Figure 1I; see the list of metabolites in Figure 1 – Source data 5, Supplementary Table 4). Approximately 84% of the metabolites that significantly differed among sorted cells also significantly differed among pipetted cells and 73% of the significant differences among pipetted samples also significantly differed among sorted samples. Of the 14 metabolites that significantly changed in sorted but not pipetted cells, 12 trended in the same direction in both sets of samples. Of the 26 metabolites that changed in pipetted but not sorted samples, 19 trended in the same direction in both sets of samples. Thus, most metabolites exhibited similar differences among AML and ALL cells irrespective of whether the cells were sorted.

To more systematically assess the similarity of pipetted and sorted samples, we plotted Log2-transformed fold change values between AML and ALL cells for all metabolites above background in sorted versus pipetted samples (Figure 1J). The slope of the regression was near 1 ($y = 0.96x – 0.06$) and the correlation was strong for most metabolites (Spearman correlation coefficient, $r = 0.81$). When we restricted the analysis to metabolites that significantly differed between sorted AML and ALL cells (fold change > 2, FDR < 0.05), the correlation was even

stronger (y = 0.95x – 0.15; r = 0.92; Figure 1K). While the levels of some metabolites did change during sorting, most metabolites strongly correlated in sorted and unsorted samples.

Effect of time on metabolite levels

It typically took up to 2 hours to sort HSCs into acetonitrile, starting from when the mice were killed. We wondered to what extent metabolite levels changed over time during cell isolation. To test this, we quickly flushed bone marrow from the long bones and made single cell suspensions in HBSS that we kept on ice. We pipetted 10,000 cell aliquots of WBM cells into acetonitrile at 5, 15, 30, 60, 120, 180, and 240 minutes after killing the mice then performed metabolomic analysis on each sample. At all time points, we detected 170 to 179 metabolites above sheath fluid background (Figure 1L). Relative to the samples collected at 5 minutes, only 2 metabolites significantly changed (fold change > 2 and FDR < 0.05) in the samples collected at 15 minutes (Figure 1M). The number of metabolites that significantly changed increased over time, but most of the changes occurred by 120 minutes (Figure 1M; see the list of metabolites that changed over time in Figure 1 - Source data 6, Supplementary Table 5). The only metabolic pathway that was significantly enriched among metabolites that changed over time was “purine metabolism” as purines were enriched in samples that incubated longer on ice. Thus, some metabolites did change over time but these represented less than 20% of detected metabolites.

To more broadly assess the similarity of the samples over time, we plotted Log2-transformed values for all detected metabolites in 5 minute versus 120 minute samples (Figure 1N). The slope of the regression was near 1 (y = 0.97x + 0.62) and the correlation was strong, r = 0.98. We also plotted non-transformed values for all detected metabolites in 5 minute versus 120 minute samples, observing a similarly high correlation (Figure 1O). Finally, to most clearly show the differences between 5 and 120 minute samples, we plotted only metabolites with signal intensity < $1x10^8$ (Figure 1P). Again, the slope of the regression was near 1 (y = 0.95x + 1.1×10^6) and the correlation was strong, r = 0.97. Thus, most metabolite intensity values

strongly correlated among samples that incubated on ice for different periods of time. However, some metabolic changes may occur within seconds of harvesting a tissue (Lu et al., 2017) in a way that was not reflected in this experiment as the 5 minute time point was the earliest at which a bone marrow cell suspension could be reliably obtained.

Effect of cell suspension buffer on metabolite levels

We typically prepare hematopoietic cell suspensions using Hanks Buffered Salt Solution (HBSS), which contains glucose. To test if this affected metabolite levels, we prepared bone marrow cell suspensions in HBSS or PBS then sorted 10,000 cells for metabolomic analysis. We detected 150 to 162 metabolites above background in these samples but only 5 significantly differed between cells isolated from HBSS versus PBS suspended samples (Figure 1 – Source data 7, Supplementary Table 6). The metabolite that most differed between these samples was glucose, which was substantially enriched in cells isolated from HBSS. Pathway enrichment analysis did not detect any pathways enriched among the metabolites that differed among HBSS and PBS samples. Therefore, the presence of glucose in the cell suspension buffer did affect glucose levels in the sorted cells but had little effect on the levels of other metabolites.

Metabolomic profiling of HSC/MPPs

To assess the metabolite profile of HSCs/MPPs we sorted 10,000 cell aliquots of $CD48^-$ $Lineage^-Sca1^+c\text{-}kit^+$ cells and WBM cells. $CD48^-Lineage^-Sca1^+c\text{-}kit^+$ cells represent 0.05% of WBM cells and are a very highly enriched for HSCs and MPPs (Oguro et al., 2013). The metabolite profiles of HSCs and MPPs are extremely similar (Agathocleous et al., 2017). We detected 160 ± 15 metabolites above sheath fluid background in HSCs/MPPs and 147 ± 15 in WBM (Figure 2A). A total of 78 metabolites significantly differed in abundance between HSCs/MPPs and WBM cells (fold change > 2 and FDR < 0.05; the metabolites are listed in Figure 2 – Source data 2, Supplementary Table 1). Of these, 51 differed by at least 2.5 fold

(Figure 2B). Of the 16 metabolites that Agathocleous et al. (Agathocleous et al., 2017) found to significantly differ between HSCs/MPPs and WBM cells, 13 also significantly differed, in the same direction, using the new method (Figure 2 - figure supplement 1). The other 3 metabolites either were not detected using the new method or could not be quantitated accurately due to extraction conditions. Thus, the new method detected most of the metabolic differences between HSC/MPPs and WBM cells observed by Agathocleous et al. (Agathocleous et al., 2017), while also detecting 65 additional differences.

Pathway enrichment analysis found only one pathway that was significantly enriched (FDR<0.01): 10 of 36 metabolites in the murine KEGG “glycerophospholipid metabolism” pathway significantly differed in abundance between HSC/MPPs and WBM cells. HSCs were enriched for many components of the Kennedy (cytidine diphosphate-choline) pathway (Li and Vance, 2008, Kennedy and Weiss, 1956), including choline, choline phosphate, CDP-choline, ethanolamine phosphate, glycerophosphorylcholine, glycerophosphorylethanolamine, and many phosphatidylcholines (PC), phosphatidylethanolamines (PE), lysophosphatidylcholines (Lyso-PC), and lysophosphatidylethanolamines (Lyso-PE) (Figure 2B - figure supplement 2). Acetylcholine and several phosphatidylserine (PS) species were depleted in HSC/MPPs as compared to WBM (Figure 2B – figure supplement 2). These results raise the possibility that glycerophospholipid synthesis is activated in HSC/MPPs relative to WBM; however, additional studies will be required in the future to test this. The prominence of phospholipids among the differences between HSCs/MPPs and WBM cells illustrates the ability of the new method to detect differences not detected by prior methods.

To determine whether metabolic perturbations in HSCs in vivo can be detected by this method, we treated mice for 3 days with methotrexate. Methotrexate inhibits dihydrofolate reductase (DHFR) and AICAR transaminase (ATIC), steps in *de novo* purine biosynthesis (Baggott et al., 1986). Methotrexate treatment did not significantly affect bone marrow cellularity or the frequencies of HSCs, MPPs, or LSK cells in the bone marrow (Figure 3A-D).

Methotrexate treatment also did not significantly affect the reconstituting potential of WBM cells upon competitive transplantation into irradiated mice (Figure 3E). Metabolomic analysis of 10,000 HSC/MPPs from the bone marrow of methotrexate-treated and control mice revealed that the only pathway that was significantly enriched among the metabolites that differed was "purine metabolism". While methotrexate would also be expected to alter folate metabolism, folate species are very difficult to detect by metabolomics (Zheng et al., 2018, Chen et al., 2017) and are not detected by our method. Given that methotrexate inhibits ATIC, AICAR levels would be expected to increase after methotrexate treatment (Cronstein et al., 1993, Baggott et al., 1986, Allegra et al., 1985). Consistent with this, AICAR levels were 88 fold higher in HSCs/MPPs from methotrexate-treated as compared to control mice (Figure 3F). The method was thus capable of detecting expected metabolic perturbations in HSCs in vivo.

Metabolomic profiling of circulating cancer cells

To test if the method is broadly applicable, we tested if we could detect metabolic differences between circulating melanoma cells from the blood and the primary subcutaneous tumors from which they arose. When efficiently metastasizing human melanomas are subcutaneously transplanted into NSG mice they spontaneously metastasize, giving rise to rare circulating melanoma cells in the blood, lymph, and metastatic tumors (Piskounova et al., 2015, Tasdogan et al., 2020, Ubellacker et al., 2020). We subcutaneously transplanted M405 patient-derived melanoma cells into NSG mice. When the subcutaneous tumors reached 2.5 cm in diameter, we isolated 10,000 cell aliquots of melanoma cells by flow cytometry from mechanically dissociated subcutaneous tumors as well as from the blood of the same mice. We pooled blood from 6-10 mice per sample to isolate 10,000 circulating melanoma cells.

We detected 145 and 154 metabolites above sheath fluid background in the subcutaneous tumor and circulating melanoma cell samples, respectively (Figure 3G). Pathway enrichment analysis of all metabolites that significantly differed between subcutaneous tumor

and circulating melanoma cells ($P < 0.05$) found one pathway that significantly (FDR < 0.01) differed, “purine metabolism”. Several purine biosynthesis intermediates were depleted in circulating melanoma cells as compared to subcutaneous tumors, including IMP, XMP, GMP, and AMP (Figure 3H-K; Figure 3 - Source data 2, Supplementary Table 1). Given that circulating melanoma cells experience high levels of oxidative stress (Piskounova et al., 2015, Tasdogan et al., 2020), these data raise the possibility that metastasizing melanoma cells reduce purine biosynthesis, and perhaps other anabolic pathways, to preserve NADPH for oxidative stress resistance.

Discussion

The method for metabolomic analysis of rare cells described in this study significantly increased metabolite numbers and pathway coverage relative to our prior method (Agathocleous et al., 2017) (Fig. 4A and 4B). We improved signal to noise ratio by using HILIC and an orbitrap mass spectrometer. We decreased contamination by eliminating sample drying and improved chromatographic performance by extracting metabolites with 80% acetonitrile. In principle, this method can be used to analyze any cell population isolated by flow cytometry, though in practice it is most useful when cell numbers are limited and when enzymatic dissociation is not required. We normalized for input variation among samples by ensuring that the average signal intensity values of metabolites detected above background were equal in the samples being compared. While it is impractical to include isotopically-labeled internal standards within the initial metabolomic analysis, since the relative levels of hundreds of different metabolites are assessed, we routinely follow-up metabolomics with other methods optimized to extract and quantitate specific metabolites of interest. In those follow-up assays we include labelled internal standards to determine absolute concentrations (Tasdogan et al., 2020, Ubellacker et al., 2020, Piskounova et al., 2015).

Cells can undergo metabolic changes upon removal from their in vivo environment (Lau et al., 2020). This is a particular problem when cells are enzymatically dissociated as they exchange metabolites with the dissociation medium, or when cells are sorted into buffers that require additional processing steps before cell lysis and metabolite extraction (Lau et al., 2020, Binek et al., 2019, Llufrio et al., 2018). To avoid changes in metabolites during cell processing, we worked quickly and kept the cells cold from the time they left the animal until they were sorted into acetonitrile. Cellular metabolism is immediately quenched by sorting into cold acetonitrile. The levels of most metabolites strongly correlated in sorted and unsorted samples (Figure 1H-K). Some metabolites exhibited changes over time during cell processing (Figure 1M) but the levels of most metabolites strongly correlated in samples at 5 and 120 minutes after removal from the mouse (Figure 1N-P). Therefore, most metabolite levels were not significantly changed by cell preparation and sorting, at least beyond 5 minutes after the mouse was killed. However, some metabolite levels might change less than a minute after the removal of cells from their normal physiological environment in a way that would not have been detected in our experiments (Lu et al., 2017). If so, it will not be possible to quantitate these metabolites in flow cytometrically isolated cells.

Transitioning to HILIC provided several advantages relative to reverse phase chromatography. We were able to avoid sample drying, which significantly reduced contamination (Figure 1B-C). We reduced ion suppression compared to our prior method because salt eluted after the metabolites of interest on HILIC columns (Figure 1F). Third, HILIC improved the separation of polar metabolites, such as central carbon metabolites, while also enabling the detection of many lipid species. Nonetheless, some metabolites are better resolved and detected by reverse phase chromatography. Therefore, while HILIC provided a net advantage for our purposes, adapting this low cell number method to other chromatographies could improve the detection of certain classes of metabolites.

Prior studies have explored many aspects of metabolomics methods, including extraction solvents and drying (Theodoridis et al., 2012). Methanol-water and acetonitrile-water mixtures have been reported to capture more metabolites than other solvents (Want et al., 2006, J et al., 2005, Bruce et al., 2008, Masson et al., 2010). Methanol is nucleophilic and can degrade metabolites with electrophilic moieties, such as nucleoside phosphates (Rabinowitz and Kimball, 2007b). Data quality and accuracy are also improved by minimizing sample manipulation after metabolite extraction, including by avoiding drying, which can promote oxidation (Siegel et al., 2014, Fan et al., 2014, Chen et al., 2017, Lu et al., 2017). We found that acetonitrile-water solvent and avoiding drying yielded the highest number of metabolites detected above sheath fluid background. HILIC resolution of metabolites was also improved when samples were injected in acetonitrile-water instead of methanol-water.

The extraction conditions we used are not suitable for the quantitation of some metabolites, including those that spontaneously oxidize (Lu et al., 2018). For example, ascorbate spontaneously oxidizes upon extraction from cells (Washko et al., 1992); therefore, in our prior study we added EDTA to the extraction solvent to prevent spontaneous oxidation (Agathocleous et al., 2017). In an effort to devise a general method in the current study, we did not add EDTA to the extraction solvent and therefore did not measure ascorbate levels accurately. Consistent with this, ascorbate was one of the 3 metabolites that differed between HSCs and WBM cells in our prior study (Agathocleous et al., 2017) that we did not detect as different in the current study (Figure 2 - figure supplement 1). The other two were spermidine and betaine, which were not detected using the new method.

We observed differences in the abundance of glycerophospholipids between HSCs/MPPs and WBM cells. Functional studies will be required to assess the biological significance of this difference. Few studies have examined lipid metabolism in HSCs (Xie et al., 2019, Ito et al., 2012, Ito et al., 2016, Lee et al., 2018, Pernes et al., 2019), partly because methods have not been readily available to quantitate lipid levels in HSCs. The ability of the new

method to detect more than 60 lipids in 10,000 HSCs may facilitate future studies of lipid metabolism in stem cells. We also performed metabolomics on circulating melanoma cells from xenografted mice. Cancer cells must undergo metabolic changes to survive oxidative stress during metastasis (Piskounova et al., 2015, Tasdogan et al., 2020). Better understanding the metabolic changes could reveal new therapeutic vulnerabilities to block cancer progression.

METHODS

Key Resources Table				
Reagent type (species) or resource	**Designation**	**Source or reference**	**Identifiers**	**Additional information**
Chemical compound, drug	Phosphate Buffered Saline Tablet	Sigma	Cat# P4417-100TAB	
Chemical compound, drug	Methanol, Optima grade for LC/MS	Fisher Scientific	Cat# A456-4	
Chemical compound, drug	Acetonitrile, Optima Grade for LCMS	Fisher Scientific	Cat# A955-4	
Chemical compound, drug	MeOH, Optima Grade for LCMS	Fisher Scientific	Cat# A456-4	
Chemical compound, drug	Water, Optima Grade for LCMS	Fisher Scientific	Cat# W6-4	
Commercial assay, kit	LS magnetic enrichment columns	Miltenyi	Cat# 130-042-401	
Commercial assay, kit	MidiMACS separator	Miltenyi	Cat# 130-042-301	
Other	Plastic microfuge tube opener	USA Scientific	Cat# 1400-1508	For minimizing metabolite contamination when opening

				microfuge tubes
Antibody	FITC anti-mouse B220, clone: RA3-6B2 (rat monoclonal)	Tonbo	Cat# 35-0452-U500, RRID:AB_2621690	Dilution: 1:400 For bone marrow HSC isolation by flow cytometry
Antibody	FITC anti-mouse Gr-1, clone: RB6-8C5 (rat monoclonal)	Tonbo	Cat# 35-5931-U500, RRID:AB 2621721	Dilution: 1:400 For bone marrow HSC isolation by flow cytometry
Antibody	FITC anti-mouse Terr119, clone: TER-119 (rat monoclonal)	Tonbo	Cat# 35-5921-U500, RRID:AB_2621720	Dilution: 1:400 For bone marrow HSC isolation by flow cytometry
Antibody	FITC anti-mouse CD2, clone: RM2-5 (rat monoclonal)	Tonbo	Cat# 35-0021-T100, RRID:AB_2621657	Dilution: 1:400 For bone marrow HSC isolation by flow cytometry
Antibody	FITC anti-mouse CD3, clone: 17A2 (rat monoclonal)	Tonbo	Cat# 35-0032-U100, RRID:AB_2621660	Dilution: 1:400 For bone marrow HSC isolation by flow cytometry
Antibody	FITC anti-mouse CD5, clone: 53-7.3 (rat monoclonal)	Biolegend	Cat# 100606, RRID:AB_312735	Dilution: 1:400 For bone marrow HSC isolation by flow cytometry
Antibody	FITC anti-mouse CD8α, clone: 53-6.7 (rat monoclonal)	Tonbo	Cat# 35-0081-U500, RRID:AB_2621671	Dilution 1:400 For bone marrow HSC isolation by flow cytometry

Antibody	APC-e780 anti-mouse c-kit, clone: 2B8 (rat monoclonal)	eBiosciences	Cat# 47-1171-82, RRID:AB_1272177	Dilution: 1:200 For bone marrow HSC isolation by flow cytometry
Antibody	PerCP-Cy5.5 anti-mouse Sca-1, clone: D7 (rat monoclonal)	BioLegend	Cat# 108124, RRID:AB_893615	Dilution 1:200
Antibody	APC anti-mouse CD48, clone: HM48-1 (Armenian hamster monoclonal)	eBiosciences	Cat# 17-0481-82, RRID:AB_469408	Dilution 1:200
Antibody	PE anti-mouse CD150, clone: TC15-12F12.2 (rat monoclonal)	BioLegend	Cat# 115904, RRID:AB_313683	Dilution 1:200
Antibody	APC anti-Mouse CD45, clone: 30-F11 (rat monoclonal)	Tonbo	Cat# 20-0451-U100, RRID:AB_2621573	Dilution 1:100
Antibody	APC anti-Mouse CD31 (PECAM-1), clone: 390 (rat monoclonal)	Biolegend	Cat# 102410, RRID:AB_312905	Dilution 1:100
Antibody	APC anti-Mouse Ter119, clone: Ter119 (rat monoclonal)	Tonbo	Cat# 20-5921-U100, RRID:AB_2621609	Dilution 1:100
Antibody	FITC anti-Human HLA-A, B, C, clone: G46-2.6 (mouse monoclonal)	BD Biosciences	Cat# 555552, RRID:AB_395935)	Dilution 1:20

Antibody	Anti-Mouse c-Kit, conjugated to para-magnetic beads, clone: 3C11 (rat monoclonal)	Miltenyi	Cat# 130-091-224, RRID:AB_2753213	(60 µl) 60 µl beads per 3x10^8 whole bone marrow cells
Antibody	Anti-Mouse CD45, conjugated to para-magnetic beads, clone: 30-F11 (rat monoclonal)	Miltenyi	Cat# 130-052-301, RRID:AB_2877061	(3 µl) 3 µl beads per 1x10^6 whole bone marrow cells
Chemical compound, drug	DAPI	Sigma-Aldrich	Cat# D8417-10mg	1 µg/ml for flow cytometry
Cell line	Human - HNT-34 AML cell line	Provided by Jian Xu's Laboratory at Children's Research Institute at UT Southwestern Medical Center. Original source: DSMZ	ACC 600, RRID: CVCL_2071	
Cell Line	Human DND-41 cell line	Provided by Jian Xu's Laboratory at Children's Research Institute at UT Southwestern Medical Center. Original source: Hui Feng, M.D./Ph.D.; Boston University	RRID: CVCL_2022	
Cell line	Human melanoma xenograft M405	Sci Trans Med 4:159ra PMCID: PMC4501487	M405	

Strain, strain background	NOD.CB17-Prkdcscid Il2rgtm1Wjl/Szj (NSG) mice	Jackson laboratories	005557, RRID:IMSR_JAX:005557	
Strain, strain background	C57BL/Ka Thy1.1 mice	Derived from Henry Kaplan's laboratory at Stanford University	N/A	
Other	ZIC-pHILIC column (2.1 x 150, 5 µm)	Millipore Sigma	Cat# 1504600001	
Software, algorithm	Omics Data Analyzer (ODA)	This manuscript	https://git.biohpc.swmed.edu/CRI/ODA	See materials and methods section "statistical analysis of metabolomics data"
Software, algorithm	Graphpad Prism V8.3	Graphpad	RRID:SCR_002798	
Software, algorithm	FlowJo V10.7.1	BD Biosciences	RRID:SCR_008520	
Software, algorithm	Freestyle V1.5	Thermo Scientific	N/A	
Software, algorithm	Trace Finder V4.0	Thermo Scientific	N/A	
Software, algorithm	Compound Discoverer V3.1	Thermo Scientific	N/A	
Chemical compound, drug	Formic Acid Optima	Fisher	Cat# A11750	
Chemical compound, drug	Ammonium acetate, Optima	Fisher	Cat# A11450	
Chemical compound, drug	Ammonium hydroxide, Optima	Fisher scientific	Cat# A470-250	

Chemical compound, drug	Methotrexate	Selleck Chem	Cat# S1210	
Chemical compound, drug	SplashMix	Avanti	Cat# 330707	

Isolation of hematopoietic cells for metabolomics

Bone marrow cells were collected quickly and maintained at 0 to 4°C throughout the staining and isolation procedure to minimize metabolic changes. Mice were euthanized by cervical dislocation. Bones were rapidly dissected and stored on ice in Hank's Buffered Salt Solution without Mg^{2+} and Ca^{2+} (HBSS, Corning). Muscle was stripped from the bones, then they were crushed in 2.5 ml of HBSS using a pre-cooled mortar and pestle, on ice. Bone marrow cells were filtered through a 40 µm strainer into a 50 ml conical tube. The cells were then stained with fluorochrome-conjugated antibodies against B220 (FITC, Tonbo), Gr-1 (FITC, Tonbo), Ter119 (FITC, Tonbo), CD2 (FITC, Tonbo), CD3 (FITC, Tonbo), CD5 (FITC, BioLegend), CD8 (FITC, Tonbo), c-kit (APC-eFluor780, eBiosciences), Sca-1 (PerCP-Cy5.5, BioLegend), CD48 (APC, eBiosciences), and CD150 (PE, BioLegend) for 30 minutes on ice. Beginning 10 minutes before adding the antibodies, and continuing after the antibodies had been added, para-magnetic beads conjugated to anti-c-kit antibodies (Miltenyi) were added to the cells to facilitate pre-enrichment of c-kit^+ cells in samples from which HSCs were sorted. To ensure that WBM cells were processed in the same way, these samples were enriched by positive selection of para-magnetic beads bound to anti-CD45 antibodies (Miltenyi). Positive selection was performed in the cold room at 4°C using a QuadroMACS manual separator (Miltenyi) and LS Columns (Miltenyi). Cells were eluted from columns in 2 ml of HBSS, centrifuged for 5 minutes at 300 x g, and resuspended in HBSS with 4',6-diamidino-2-phenylindole (DAPI, 1 µg/ml, Sigma) for flow cytometry. The gating strategy for the isolation of HSCs/MPPs is depicted in Figure 3 – figure supplement 2A.

Isolation of melanoma cells for metabolomics

Mice were transplanted subcutaneously with human melanoma cells and the cells were allowed to spontaneously metastasize until the subcutaneous tumors reached 2.5 cm. At this point, single cell suspensions were obtained by dissociating tumors mechanically with a scalpel on ice followed by gentle trituration. Cells were filtered through a 40 μm strainer to generate a single cell suspension. Blood was collected from mice by cardiac puncture with a syringe pretreated with citrate-dextrose solution (Santa Cruz).

Subcutaneous tumor and blood specimens were first incubated on ice for 10 minutes with Ammonium-Chloride-Potassium (ACK) lysing buffer to eliminate red blood cells. The cells were washed with PBS and then stained with antibodies prior to flow cytometry. All antibody staining was performed for 20 minutes on ice, followed by washing with PBS and centrifuging at 200 x g for 5 minutes. Cells were stained with directly conjugated antibodies against mouse CD45 (APC, Tonbo Biosciences), mouse CD31 (APC, Biolegend), mouse Ter119 (APC, Tonbo Biosciences) and human HLA-A, B, C (G46-2.6-FITC, BD Biosciences). Human melanoma cells were isolated as cells that were positive for HLA and DsRed (melanoma cells were tagged with constitutive DsRed before subcutaneous transplantation), and negative for mouse endothelial (CD31) and hematopoietic markers (CD45 and Ter119). Cells were washed with PBS and resuspended in DAPI (1 μg/ml, Sigma) to eliminate dead cells from sorts and analyses. The flow cytometry gating strategies for the isolation of primary tumor cells and circulating melanoma cells are depicted in Figure 3 – figure supplement 2B-C.

Cell lines

Human HNT-34 (DSMZ Cat # ACC 600, RRID: CVCL_2071) and Human DND-41 (Hui Feng, M.D./Ph.D.; Boston University, RRID: CVCL_2022) cell lines were provided by Jian Xu's laboratory at Children's Research Institute at UT Southwestern. To confirm the identity of these

cell lines, we performed qRT-PCR and Western Blot analyses of several leukemia signature genes (Ng et al., 2016). We also performed RNA-seq and whole genome sequencing and compared the results with previous studies. All cell lines tested negative for mycoplasma contamination using the Lonza MycoAlert kit (Lonza # LT07-118). No cell lines used in this study were found in the database of commonly misidentified cell lines maintained by the International Cell Line Authentication Committee (ICLAC) or the National Center for Biotechnology Information (NCBI) BioSample.

Sorting versus pipetting of cultured cells for metabolomics

HNT-34 AML cells and DND-41 T-ALL cells were cultured non-adherently in RPMI with 10% fetal bovine serum and 1% penicillin/streptomycin. Cells were maintained at a density of $5x10^5$ cells/ml, and cultured at 37°C with 5% CO_2. AML or ALL cells were removed from the incubator and centrifuged at 4°C to pellet the cells, then resuspended in ice-cold PBS and centrifuged again, before being resuspended in ice cold PBS at a density of $1x10^6$ cells/ml. 10 µl of the AML or ALL cell suspension was then pipetted into 40 µl of 100% acetonitrile to create a final metabolite extract of 10,000 cells in 50 µl 80% acetonitrile (10 minutes total processing time). 10,000 AML or ALL cells from the same cell suspensions were also sorted into 40 µl of 100% acetonitrile to create a final metabolite extract of 10,000 cells in 50 µl of 80% acetonitrile (30 to 60 minutes processing time). The cells were kept ice cold before and during sorting.

Flow cytometer preparation

Flow cytometers were thoroughly cleaned before sorting low abundance samples to minimize background. All flow cytometry was performed using a FACSAria II or a FACSAria Fusion (BD Biosciences). The fluidics shutdown protocols were performed using 80% ethanol before each sort. A clean, metabolomics-dedicated FACSAria sheath tank was rinsed with ultrapure water several times to reduce contamination, before being filled with 4 l of 0.5x

phosphate buffered saline (PBS) made from tablets (Sigma) dissolved in ultrapure water. The metabolomics sheath tank was connected to the sorter using a dedicated 0.22 µm filter. The fluidics startup protocol was performed using freshly made 0.5x PBS sheath fluid. The sorter was configured to use a 70 µm nozzle but before the nozzle was inserted two cycles of clean flow cell protocols were performed with Windex. The sheath fluid was then run through the flow cytometer without a nozzle for 5 minutes to flush Windex and any remaining debris from the flow cell. At the same time, the 70 µm nozzle was sonicated for 5 minutes to remove contamination and debris, and the cleanliness of the nozzle was confirmed by microscopy. The sheath fluid stream was turned off and the sort chamber was cleaned with a lint-free wipe and cotton swabs. The nozzle was then inserted and the stream was turned on. The sample line was cleaned again by running a 5 ml sample tube of Windex for 5 minutes, followed by ultrapure water for 5 minutes. Four-way purity sort mode was used to minimize droplet size. The cell sample, the sorting chamber, and the collection tube adapter were all maintained at 4°C during sorting.

Sorting cells for metabolomics

The Eppendorf tubes into which cells were sorted were loaded with 40 µl of 100% acetonitrile (Optima, Fisher Scientific) or methanol (Optima, Fisher Scientific) before sorting. We used a freshly opened bag of clean Eppendorf tubes (USA Scientific) and filtered pipette tips. The Eppendorf tubes were maintained at -20°C until just prior to sorting. Cell samples were filtered through a 40 µm strainer before sorting. The flow rate was minimized to reduce shear stress. Just before sorting, the Eppendorf tubes were opened using a clean microfuge tube opener (USA Scientific) to avoid contamination. After sorting, the tubes were sealed, vortexed and centrifuged briefly to collect all the liquid in the bottom of the tube, and placed on dry ice. Metabolites were extracted by vortexing again for 1 minute at high speed, followed by centrifugation at 17,000 x g for 15 minutes at 4°C. The supernatant was transferred to auto-sampler vials with low volume inserts and analyzed immediately by LC-MS (see details below).

Liquid chromatography and mass spectrometry

Liquid chromatography was performed with a Vanquish Flex UHPLC (Thermo Scientific). The reverse phase method used a Waters HSS C18 column (2.1 x 150 mm, 1.7 µm) with a binary solvent gradient. Mobile phase A was water with 0.1% formic acid and mobile phase B was acetonitrile with 0.1% formic acid. Gradient separation proceeded as follows: from 0 to 5 minutes, 0% B; from 5 minutes to 45 minutes mobile phase B was ramped linearly from 0% to 100%; from 45 minutes to 52 minutes, mobile phase B was held at 100%; from 52 to 52.1 minutes, mobile phase B was ramped linearly to 0%; from 52.1 to 60 minutes, mobile phase B was held at 0%. Throughout the course of the method, the solvent flow rate was kept to 100 µl/minute and column temperature was held at 30°C.

The HILIC method used a Millipore Sigma ZIC-pHILIC column (2.1 x 150, 5 µm) with a binary solvent gradient. Mobile phase A was water containing 10 mM ammonium acetate, pH 9.8 with ammonium hydroxide; mobile phase B was 100% acetonitrile. Gradient separation proceeded as follows: from 0 to 15 minutes mobile phase B was ramped linearly from 90% to 30%; from 15 minutes to 18 minutes, mobile phase B was held at 30%; from 18 minutes to 19 minutes, mobile phase B was ramped linearly from 30% to 90%; mobile phase B was held at 90% from 19 minutes to 27 minutes to regenerate the initial chromatographic environment. Throughout the method, solvent flow rate was kept at 250 µl/minute and the column temperature was maintained at 25°C. For low abundance samples, 20 µl of sample was injected onto the column. For high abundance samples, 10 µl was injected.

All mass spectrometry data were acquired using a Thermo Scientific (Bremen, Germany) QExactive HF-X mass spectrometer (LC-MS/MS). For low abundance samples, polarity-switching MS1 only acquisition was used. Each polarity was acquired at a resolving power of 120,000 full width at half maximum (FWHM); the automatic gain control (AGC) target was set to 1,000,000 with a maximum inject time of 50 milliseconds. The scan range was set to 80-1200

Daltons. High-abundance samples analyzed for library construction were acquired with two separate ddMS2 methods – one for positive mode and another for negative mode. Precursor MS1 data for this method were acquired with the exact same settings as those described above. Product ion MS data were acquired with a resolving power of 15,000 FWHM; the AGC target was set to 200,000, with a maximum inject time of 150 ms. A top-10 data dependent MS scheme was used with an isolation window of 1 Da and an isolation offset of 0.5 Da. Analytes were fragmented with stepped collision energies of 30, 50 and 70 Normalized Collision Energy (NCE) units. The minimum AGC target was 8,000 with a dynamic exclusion of 30 seconds.

Instrument performance was evaluated before each experiment by analyzing a quality control sample, 20ul of freshly-obtained rat serum. We compared peak areas of individual metabolites and the total number of metabolites detected in the control sample with control samples run in prior experiments. If the peak area values and total metabolite identifications fell outside of 1 standard deviation from the historical average, the instrument was cleaned to re-optimize sensitivity.

Metabolite library development

To develop the metabolite library we used to analyze samples, we acquired LC-MS/MS data from high abundance samples using a data dependent MS/MS method. Metabolites were identified in an unbiased fashion using Compound Discoverer 3.0 (ThermoScientific). Metabolites were added to the initial library only if they met the following criteria. First, chromatographic peaks had to align in all samples, and peak intensity had to increase with cell number. Second, precursor mass accuracy had to be within 5 ppm of theoretical mass, with an naturally occurring isotope pattern that matched that predicted by the chemical formula. Third, the MS/MS product ion spectra had to either match an annotated database (mzCloud, Human Metabolome Data Base, Lipid Maps, and ChemSpider) or had to be confirmed by analysis of chemical standards. This process yielded a 590 metabolite library with known masses and

chromatographic retention times. This library was imported into the manual peak review software Trace Finder 4.1 (ThermoScientific) for manual peak integration of all low abundance LC-MS data. To narrow this list of 590 metabolites to the metabolites that might be detected in 10,000 sorted cells, we determined which of the 590 metabolites were observed in 100,000 WBM cells. We found 289 metabolites that were detected in 100,000 WBM cells. This 289 metabolite library was used for manual analyses of LC-MS data from low abundance samples. When additional metabolites were observed in new experiments they were added to the library.

Melanoma specimens

Melanoma specimens were obtained with informed consent from all patients according to protocols approved by the Institutional Review Board (IRB) of the University of Michigan Medical School (IRBMED approvals HUM00050754 and HUM00050085 (Quintana et al., 2012)) and the University of Texas Southwestern Medical Center (IRB approval 102010-051). Materials used in the manuscript are available, though there are restrictions imposed by IRB requirements and institutional policy on the sharing of materials from patients.

Mouse studies and xenograft assays

All mouse experiments complied with all relevant ethical regulations and were performed according to protocols approved by the Institutional Animal Care and Use Committee at the University of Texas Southwestern Medical Center (protocols 2016-101360 and 2019-102632). For all experiments, mice were kept on normal chow and fed *ad libitum*. The mice used in all experiments were 8 to 12 week-old C57BL/Ka mice, with the exception of melanoma studies, which were subcutaneously xenografted into 4 to 8 week-old NOD.CB17-*Prkdc*^{scid} *Il2rg*^{tm1Wjl}/SzJ (NSG) mice. Both male and female mice were used. For melanoma experiments, the maximum permitted tumor diameter was 2.5 cm. Subcutaneous tumor diameters were measured weekly with calipers until any tumor in the mouse cohort reached 2.5 cm in its largest diameter. At that

point, all mice in the cohort were killed, per approved protocol, for analysis of subcutaneous tumors and circulating melanoma cells. For each replicate, subcutaneous tumors and circulating melanoma cells were pooled from 6-10 mice.

Methotrexate treatment

8-12 week old C57BL/Ka mice were intraperitoneally injected daily with methotrexate (1.25 mg/kg/day) or DMSO control, for 3 days. Mice were sacrificed by cervical dislocation 2 hours after the final methotrexate dose and bone marrow cells were collected for analysis.

Statistical analysis of metabolomic data

We developed an R tool for the analysis of metabolite LC-MS peak intensity data. The data were visualized using multiple methods, including violin-box plots, histograms, clustered heatmaps, principle component analysis, and correlation plots to assess data quality and identify batch effects. To assess the statistical significance of differences in metabolite levels between samples we used R's Generalized Linear Models (GLM) (Dobson and Barnett, 2018) function with the Gaussian distribution on log-transformed data. To compare metabolite levels in cell samples to sheath fluid samples we used GLM with $\log_2(x+1)$-transformed, non-normalized data. Metabolites with fold change > 2 and FDR < 0.05 were considered above background. To assess the statistical significance of differences in metabolite levels between two types of cells, we normalized the cell samples using the Relative Log Expression (RLE) method (Anders and Huber, 2010), and $\log_2$-transformed the normalized data. For all comparisons between samples, we used the half-minimum imputation to replace zero values with half of the minimum non-zero value for each metabolite, and used R's GLM method. To adjust for multiple comparisons we used the False Discovery Rate (FDR) method. For comparisons between different cell samples, we used fold change > 2 and FDR < 0.05 as cutoffs for statistical significance. When samples (such as HSCs and WBM cells) were from the same mice we used pairing as an independent

variable in the GLM. When batch effects were observed, we used batch as an independent variable in the GLM. R packages used by this tool include stats, openxlsx, data.table, gtools, matrixStats, cplm, ggplot2, cowplot, pheatmap, ggcorrplot, eulerr, and GGally.

The metabolomics data analysis tool can be downloaded from https://git.biohpc.swmed.edu/CRI/ODA for academic use. This tool includes an ODA.R script file, an accompanying Excel data template file, and example analyses. The script can be run from Linux/MacIntosh Terminal or Windows PowerShell using the Rscript command followed by the Excel input file name and the Excel output file name. R with the Rscript command (version 3.5.1 or later is recommended) and internet access are required to run this tool as other R packages must be auto-downloaded by the tool. Data should be entered into the Excel template and parameters for analysis selected. First-time users should read the instructions in the data template. The analysis reports and figures are saved together in the Excel output file. Figures are also saved in a folder in the .png and .ps formats. Example analysis results are provided to illustrate typical analysis settings and their outputs.

Assessing statistical significance

Mice were allocated to experiments randomly and samples processed in an arbitrary order, but formal randomization techniques were not used. Prior to analyzing the statistical significance of differences among treatments, we tested whether the data were normally distributed and whether variance was similar among treatments. To test for normal distribution, we performed the Shapiro–Wilk test when $3 \leq n < 20$ or the D'Agostino Omnibus test when $n \geq 20$. To test if variability significantly differed among treatments, we performed *F*-tests (for experiments with two treatments) or Levene's median tests (for more than two treatments). When the data significantly deviated from normality or variability significantly differed among treatments, we log2-transformed the data and tested again for normality and variability. If the

transformed data did not significantly deviate from normality and equal variability, we performed parametric tests on the transformed data. Fold change data were always log2-transformed.

All the statistical tests we used were two-sided, where applicable. To assess the statistical significance of a difference between two treatments, we used Student's t-tests or paired t-tests (when a parametric test was appropriate). To assess the statistical significance of differences between two cumulative frequency distributions, we used the Kolmogorov–Smirnov tests. Multiple Kolmogorov–Smirnov tests were followed by Holm-Sidak's multiple comparisons adjustment. To assess the statistical significance of differences between more than two treatments, we used paired sample one-way or two-way ANOVAs (when a parametric test was appropriate) followed by Tukey's, Dunnet's, or Sidak's multiple comparisons adjustment. To assess the statistical significance of differences between transplant data, we used mixed-effects analysis (when a parametric test was appropriate and there were missing data points) followed by Sidak's multiple comparisons adjustment. To assess the correlation between two sets of samples, we calculated Spearman correlation coefficients (r, the data were not normally distributed) and performed linear regression analysis.

All statistical analyses were performed with Graphpad Prism 8.3. All data represent mean ± standard deviation. Samples sizes were not pre-determined based on statistical power calculations but were based on our experience with these assays. No data were excluded; however, mice sometimes died during experiments, presumably due to complications associated with irradiation and bone marrow transplantation. In those instances, data that had already been collected on the mice in interim analyses were included (such as donor contribution to peripheral blood chimerism over time).

References

Abouleila, Y., Onidani, K., Ali, A., Shoji, H., Kawai, T., Lim, C. T., Kumar, V., Okaya, S., Kato, K., Hiyama, E., Yanagida, T., Masujima, T., Shimizu, Y. & Honda, K. 2019. Live single

cell mass spectrometry reveals cancer-specific metabolic profiles of circulating tumor cells. *Cancer Sci,* 110**,** 697-706.

Agathocleous, M., Meacham, C. E., Burgess, R. J., Piskounova, E., Zhao, Z., Crane, G. M., Cowin, B. L., Bruner, E., Murphy, M. M., Chen, W., Spangrude, G. J., Hu, Z., Deberardinis, R. J. & Morrison, S. J. 2017. Ascorbate regulates haematopoietic stem cell function and leukaemogenesis. *Nature,* 549**,** 476-481.

Ali, A., Abouleila, Y., Shimizu, Y., Hiyama, E., Emara, S., Mashaghi, A. & Hankemeier, T. 2019. Single-cell metabolomics by mass spectrometry: Advances, challenges, and future applications. *TrAC Trends in Analytical Chemistry,* 120**,** 115436.

Allegra, C. J., Drake, J. C., Jolivet, J. & Chabner, B. A. 1985. Inhibition of phosphoribosylaminoimidazolecarboxamide transformylase by methotrexate and dihydrofolic acid polyglutamates. *Proceedings of the National Academy of Sciences of the United States of America,* 82**,** 4881-4885.

Anders, S. & Huber, W. 2010. Differential expression analysis for sequence count data. *Genome Biology,* 11**,** R106.

Ansó, E., Weinberg, S. E., Diebold, L. P., Thompson, B. J., Malinge, S., Schumacker, P. T., Liu, X., Zhang, Y., Shao, Z., Steadman, M., Marsh, K. M., Xu, J., Crispino, J. D. & Chandel, N. S. 2017. The mitochondrial respiratory chain is essential for haematopoietic stem cell function. *Nature cell biology,* 19**,** 614-625.

Baggott, J. E., Vaughn, W. H. & Hudson, B. B. 1986. Inhibition of 5-aminoimidazole-4-carboxamide ribotide transformylase, adenosine deaminase and 5'-adenylate deaminase by polyglutamates of methotrexate and oxidized folates and by 5-aminoimidazole-4-carboxamide riboside and ribotide. *Biochem J,* 236**,** 193-200.

Binek, A., Rojo, D., Godzien, J., Rupérez, F. J., Nuñez, V., Jorge, I., Ricote, M., Vázquez, J. & Barbas, C. 2019. Flow Cytometry Has a Significant Impact on the Cellular Metabolome. *J Proteome Res,* 18**,** 169-181.

Bruce, S. J., Jonsson, P., Antti, H., Cloarec, O., Trygg, J., Marklund, S. L. & Moritz, T. 2008. Evaluation of a protocol for metabolic profiling studies on human blood plasma by combined ultra-performance liquid chromatography/mass spectrometry: From extraction to data analysis. *Anal Biochem,* 372**,** 237-49.

Chen, L., Ducker, G. S., Lu, W., Teng, X. & Rabinowitz, J. D. 2017. An LC-MS chemical derivatization method for the measurement of five different one-carbon states of cellular tetrahydrofolate. *Anal Bioanal Chem,* 409**,** 5955-5964.

Comi, T. J., Do, T. D., Rubakhin, S. S. & Sweedler, J. V. 2017. Categorizing Cells on the Basis of their Chemical Profiles: Progress in Single-Cell Mass Spectrometry. *Journal of the American Chemical Society,* 139**,** 3920-3929.

Cronstein, B. N., Naime, D. & Ostad, E. 1993. The antiinflammatory mechanism of methotrexate. Increased adenosine release at inflamed sites diminishes leukocyte accumulation in an in vivo model of inflammation. *The Journal of clinical investigation,* 92**,** 2675-2682.

Dobson, A. J. & Barnett, A. G. 2018. *An introduction to generalized linear models*, CRC press.

Duncan, K. D., Fyrestam, J. & Lanekoff, I. 2019. Advances in mass spectrometry based single-cell metabolomics. *Analyst,* 144**,** 782-793.

Evers, T. M. J., Hochane, M., Tans, S. J., Heeren, R. M. A., Semrau, S., Nemes, P. & Mashaghi, A. 2019. Deciphering Metabolic Heterogeneity by Single-Cell Analysis. *Analytical Chemistry,* 91**,** 13314-13323.

Fan, J., Ye, J., Kamphorst, J. J., Shlomi, T., Thompson, C. B. & Rabinowitz, J. D. 2014. Quantitative flux analysis reveals folate-dependent NADPH production. *Nature,* 510**,** 298-302.

Hiyama, E., Ali, A., Amer, S., Harada, T., Shimamoto, K., Furushima, R., Abouleila, Y., Emara, S. & Masujima, T. 2015. Direct Lipido-Metabolomics of Single Floating Cells for Analysis

of Circulating Tumor Cells by Live Single-cell Mass Spectrometry. *Analytical Sciences,* 31**,** 1215-1217.

Ito, K., Carracedo, A., Weiss, D., Arai, F., Ala, U., Avigan, D. E., Schafer, Z. T., Evans, R. M., Suda, T., Lee, C. H. & Pandolfi, P. P. 2012. A PML–PPAR-δ pathway for fatty acid oxidation regulates hematopoietic stem cell maintenance. *Nat Med,* 18**,** 1350-8.

Ito, K., Turcotte, R., Cui, J., Zimmerman, S. E., Pinho, S., Mizoguchi, T., Arai, F., Runnels, J. M., Alt, C., Teruya-Feldstein, J., Mar, J. C., Singh, R., Suda, T., Lin, C. P., Frenette, P. S. & Ito, K. 2016. Self-renewal of a purified Tie2+ hematopoietic stem cell population relies on mitochondrial clearance. *Science,* 354**,** 1156.

Ito, K., Bonora, M. & Ito, K. 2019. Metabolism as master of hematopoietic stem cell fate. *Int J Hematol,* 109**,** 18-27.

J, A., Trygg, J., Gullberg, J., Johansson, A. I., Jonsson, P., Antti, H., Marklund, S. L. & Moritz, T. 2005. Extraction and GC/MS Analysis of the Human Blood Plasma Metabolome. *Anal Chem,* 77**,** 8086-8094.

Jang, C., Chen, L. & Rabinowitz, J. D. 2018. Metabolomics and Isotope Tracing. *Cell,* 173**,** 822-837.

Karigane, D., Kobayashi, H., Morikawa, T., Ootomo, Y., Sakai, M., Nagamatsu, G., Kubota, Y., Goda, N., Matsumoto, M., Nishimura, Emi k., Soga, T., Otsu, K., Suematsu, M., Okamoto, S., Suda, T. & Takubo, K. 2016. p38α Activates Purine Metabolism to Initiate Hematopoietic Stem/Progenitor Cell Cycling in Response to Stress. *Cell Stem Cell,* 19**,** 192-204.

Kennedy, E. P. & Weiss, S. B. 1956. The function of cytidine coenzymes in the biosynthesis of phospholipides. *J Biol Chem,* 222**,** 193-214.

Kim, J. & Deberardinis, R. J. 2019. Mechanisms and Implications of Metabolic Heterogeneity in Cancer. *Cell Metabolism,* 30**,** 434-446.

Lau, A. N., Li, Z., Danai, L. V., Westermark, A. M., Darnell, A. M., Ferreira, R., Gocheva, V., Sivanand, S., Lien, E. C., Sapp, K. M., Mayers, J. R., Biffi, G., Chin, C. R., Davidson, S. M., Tuveson, D. A., Jacks, T., Matheson, N. J., Yilmaz, O. & Vander Heiden, M. G. 2020. Dissecting cell type-specific metabolism in pancreatic ductal adenocarcinoma. *eLife,* 9**,** e56782.

Lee, M. K. S., Al-Sharea, A., Dragoljevic, D. & Murphy, A. J. 2018. Hand of FATe: lipid metabolism in hematopoietic stem cells. *Current Opinion in Lipidology,* 29.

Li, Z. & Vance, D. E. 2008. Thematic Review Series: Glycerolipids. Phosphatidylcholine and choline homeostasis. *Journal of Lipid Research,* 49**,** 1187-1194.

Li, Z., Wang, Z., Tang, Y., Lu, X., Chen, J., Dong, Y., Wu, B., Wang, C., Yang, L., Guo, Z., Xue, M., Lu, S., Wei, W. & Shi, Q. 2019. Liquid biopsy-based single-cell metabolic phenotyping of lung cancer patients for informative diagnostics. *Nature Communications,* 10**,** 3856.

Llufrio, E. M., Wang, L., Naser, F. J. & Patti, G. J. 2018. Sorting cells alters their redox state and cellular metabolome. *Redox Biol,* 16**,** 381-387.

Lu, W., Su, X., Klein, M. S., Lewis, I. A., Fiehn, O. & Rabinowitz, J. D. 2017. Metabolite Measurement: Pitfalls to Avoid and Practices to Follow. *Annual review of biochemistry,* 86**,** 277-304.

Lu, W., Wang, L., Chen, L., Hui, S. & Rabinowitz, J. D. 2018. Extraction and Quantitation of Nicotinamide Adenine Dinucleotide Redox Cofactors. *Antioxid Redox Signal,* 28**,** 167-179.

Luo, X. & Li, L. 2017. Metabolomics of Small Numbers of Cells: Metabolomic Profiling of 100, 1000, and 10000 Human Breast Cancer Cells. *Analytical Chemistry,* 89**,** 11664-11671.

Masson, P., Alves, A. C., Ebbels, T. M. D., Nicholson, J. K. & Want, E. J. 2010. Optimization and Evaluation of Metabolite Extraction Protocols for Untargeted Metabolic Profiling of Liver Samples by UPLC-MS. *Anal Chem,* 82**,** 7779-7786.

Micalizzi, D. S., Maheswaran, S. & Haber, D. A. 2017. A conduit to metastasis: circulating tumor cell biology. *Genes & development,* 31**,** 1827-1840.

Muir, A., Danai, L. V. & Vander Heiden, M. G. 2018. Microenvironmental regulation of cancer cell metabolism: implications for experimental design and translational studies. *Dis Model Mech,* 11**,** dmm035758.

Naka, K., Jomen, Y., Ishihara, K., Kim, J., Ishimoto, T., Bae, E. J., Mohney, R. P., Stirdivant, S. M., Oshima, H., Oshima, M., Kim, D. W., Nakauchi, H., Takihara, Y., Kato, Y., Ooshima, A. & Kim, S. J. 2015. Dipeptide species regulate p38MAPK-Smad3 signalling to maintain chronic myelogenous leukaemia stem cells. *Nat Commun,* 6**,** 8039.

Nemes, P., Knolhoff, A. M., Rubakhin, S. S. & Sweedler, J. V. 2012. Single-cell metabolomics: changes in the metabolome of freshly isolated and cultured neurons. *ACS Chem Neurosci,* 3**,** 782-792.

Ng, S. W. K., Mitchell, A., Kennedy, J. A., Chen, W. C., Mcleod, J., Ibrahimova, N., Arruda, A., Popescu, A., Gupta, V., Schimmer, A. D., Schuh, A. C., Yee, K. W., Bullinger, L., Herold, T., Görlich, D., Büchner, T., Hiddemann, W., Berdel, W. E., Wörmann, B., Cheok, M., Preudhomme, C., Dombret, H., Metzeler, K., Buske, C., Löwenberg, B., Valk, P. J. M., Zandstra, P. W., Minden, M. D., Dick, J. E. & Wang, J. C. Y. 2016. A 17-gene stemness score for rapid determination of risk in acute leukaemia. *Nature,* 540**,** 433-437.

Oguro, H., Ding, L. & Morrison, S. J. 2013. SLAM family markers resolve functionally distinct subpopulations of hematopoietic stem cells and multipotent progenitors. *Cell stem cell,* 13**,** 102-116.

Onjiko, R. M., Moody, S. A. & Nemes, P. 2015. Single-cell mass spectrometry reveals small molecules that affect cell fates in the 16-cell embryo. *Proceedings of the National Academy of Sciences of the United States of America,* 112**,** 6545-6550.

Pernes, G., Flynn, M. C., Lancaster, G. I. & Murphy, A. J. 2019. Fat for fuel: lipid metabolism in haematopoiesis. *Clin Transl Immunology,* 8**,** e1098-e1098.

827 Piskounova, E., Agathocleous, M., Murphy, M. M., Hu, Z., Huddlestun, S. E., Zhao, Z., Leitch, A.
828 M., Johnson, T. M., Deberardinis, R. J. & Morrison, S. J. 2015. Oxidative stress inhibits
829 distant metastasis by human melanoma cells. *Nature,* 527**,** 186-91.
830 Quintana, E., Piskounova, E., Shackleton, M., Weinberg, D., Eskiocak, U., Fullen, D. R.,
831 Johnson, T. M. & Morrison, S. J. 2012. Human Melanoma Metastasis in NSG Mice
832 Correlates with Clinical Outcome in Patients. *Science Translational Medicine,* 4**,**
833 159ra149.
834 Rabinowitz, J. D. & Kimball, E. 2007a. Acidic Acetonitrile for Cellular Metabolome Extraction
835 from Escherichia coli. *Analytical Chemistry,* 79**,** 6167-6173.
836 Rabinowitz, J. D. & Kimball, E. H. 2007b. Acidic Acetonitrile for Cellular Metabolome Extraction
837 from Escherichia coli. *Anal Chem,* 79**,** 6167-6173.
838 Siegel, D., Permentier, H., Reijngoud, D. J. & Bischoff, R. 2014. Chemical and technical
839 challenges in the analysis of central carbon metabolites by liquid-chromatography mass
840 spectrometry. *J Chromatogr B Analyt Technol Biomed Life Sci,* 966**,** 21-33.
841 Simsek, T., Kocabas, F., Zheng, J., Deberardinis, R. J., Mahmoud, A. I., Olson, E. N.,
842 Schneider, J. W., Zhang, C. C. & Sadek, H. A. 2010. The distinct metabolic profile of
843 hematopoietic stem cells reflects their location in a hypoxic niche. *Cell Stem Cell,* 7**,** 380-
844 90.
845 Takubo, K., Nagamatsu, G., Kobayashi, Chiharu i., Nakamura-Ishizu, A., Kobayashi, H., Ikeda,
846 E., Goda, N., Rahimi, Y., Johnson, Randall s., Soga, T., Hirao, A., Suematsu, M. &
847 Suda, T. 2013. Regulation of Glycolysis by Pdk Functions as a Metabolic Checkpoint for
848 Cell Cycle Quiescence in Hematopoietic Stem Cells. *Cell Stem Cell,* 12**,** 49-61.
849 Tasdogan, A., Faubert, B., Ramesh, V., Ubellacker, J. M., Shen, B., Solmonson, A., Murphy, M.
850 M., Gu, Z., Gu, W., Martin, M., Kasitinon, S. Y., Vandergriff, T., Mathews, T. P., Zhao, Z.,
851 Schadendorf, D., Deberardinis, R. J. & Morrison, S. J. 2020. Metabolic heterogeneity
852 confers differences in melanoma metastatic potential. *Nature,* 577**,** 115-120.

Theodoridis, G. A., Gika, H. G., Want, E. J. & Wilson, I. D. 2012. Liquid chromatography-mass spectrometry based global metabolite profiling: a review. *Anal Chim Acta,* 711**,** 7-16.

Ubellacker, J. M., Tasdogan, A., Ramesh, V., Shen, B., Mitchell, E. C., Martin-Sandoval, M. S., Gu, Z., Mccormick, M. L., Durham, A. B., Spitz, D. R., Zhao, Z., Mathews, T. P. & Morrison, S. J. 2020. Lymph protects metastasizing melanoma cells from ferroptosis. *Nature,* 585**,** 113-118.

Wang, Y. H., Israelsen, W. J., Lee, D., Yu, V. W., Jeanson, N. T., Clish, C. B., Cantley, L. C., Vander Heiden, M. G. & Scadden, D. T. 2014. Cell-state-specific metabolic dependency in hematopoiesis and leukemogenesis. *Cell,* 158**,** 1309-23.

Want, E., O'maille, G., Smith, C., Brandon, T., Wilasinee, U., Qin, C., Trauger, S. & Siuzdak, G. 2006. Solvent-Dependent Metabolite Distribution, Clustering, and Protein Extraction for Serum Profiling with Mass Spectrometry. *Anal Chem,* 78**,** 743-752.

Washko, P. W., Welch, R. W., Dhariwal, K. R., Wang, Y. & Levine, M. 1992. Ascorbic acid and dehydroascorbic acid analyses in biological samples. *Analytical Biochemistry,* 204**,** 1-14.

Xie, S. Z., Garcia-Prat, L., Voisin, V., Ferrari, R., Gan, O. I., Wagenblast, E., Kaufmann, K. B., Zeng, A. G. X., Takayanagi, S.-I., Patel, I., Lee, E. K., Jargstorf, J., Holmes, G., Romm, G., Pan, K., Shoong, M., Vedi, A., Luberto, C., Minden, M. D., Bader, G. D., Laurenti, E. & Dick, J. E. 2019. Sphingolipid Modulation Activates Proteostasis Programs to Govern Human Hematopoietic Stem Cell Self-Renewal. *Cell stem cell,* 25**,** 639-653.e7.

Zheng, Y., Lin, T. Y., Lee, G., Paddock, M. N., Momb, J., Cheng, Z., Li, Q., Fei, D. L., Stein, B. D., Ramsamooj, S., Zhang, G., Blenis, J. & Cantley, L. C. 2018. Mitochondrial One-Carbon Pathway Supports Cytosolic Folate Integrity in Cancer Cells. *Cell,* 175**,** 1546-1560.e17.

878 **Acknowledgements**

879 S.J.M. is a Howard Hughes Medical Institute (HHMI) Investigator, the Mary McDermott Cook
880 Chair in Pediatric Genetics, the Kathryn and Gene Bishop Distinguished Chair in Pediatric
881 Research, the director of the Hamon Laboratory for Stem Cells and Cancer, and a Cancer
882 Prevention and Research Institute of Texas Scholar. A.W.D was supported by a Ruth L.
883 Kirschstein NRSA Fellowship. A.T. was supported by the Leopoldina Fellowship Program
884 (LPDS 2016-16) of the German National Academy of Sciences and the Fritz Thyssen
885 Foundation. This work was also funded by the National Institutes of Health (DK11875 and
886 CA228608) and the Cancer Prevention and Research Institute of Texas (RP180778). Jian Xu
887 provided the AML and ALL cell lines used in this study. The BioHPC high performance
888 computing cloud at UTSW was used for data analysis and storage as well as metabolomics
889 data analysis (ODA) software deployment. The Moody Foundation Flow Cytometry Core was
890 used for all flow cytometry. The graphic in Figure 4B was created using BioRender
891 (BioRender.com).

892

893 **Corresponding Author**

894 Correspondence and requests for materials should be addressed to Sean J. Morrison.
895 (Sean.Morrison@UTSouthwestern.edu) or Thomas P, Matthews
896 (Thomas.Mathews@UTSouthwestern.edu).

897

898 **Author Declarations**

899 S.J.M. is an advisor for Frequency Therapeutics and Protein Fluidics as well as a stockholder in
900 G1 Therapeutics.

901

902 **FIGURE LEGENDS**

903 **Figure 1: Sample processing and chromatography parameters.**

(A) The number of metabolites identified with high confidence spectral database matching in WBM samples after HILIC or reverse phase chromatography (n = 3 replicates per group from one experiment). **(B)** Average peak intensities in sheath fluid background samples after drying with a standard vacuum concentrator, a vacuum concentrator in a positive pressure HEPA-filtered clean hood, or with no drying (n = 5 replicates per treatment from one experiment). **(C)** Number of metabolites significantly above sheath fluid background in 10,000 sorted WBM cells after drying with a standard vacuum concentrator, a vacuum concentrator in a clean hood, or with no drying (n = 5 replicates per treatment from one experiment). The threshold for statistical significance relative to background or other samples was always set at fold change > 2 and FDR < 0.05, unless otherwise indicated. **(D)** Metabolites detected in 100,000 WBM cells extracted with 80% acetonitrile in water (ACN), 80% methanol in water (MeOH), or 40% ACN plus 40% MeOH in water (Mix) (n = 3 replicates per treatment from one experiment). (**E)** Overlap in metabolites detected with each extraction solvent (n = 3 replicates per treatment from one experiment). **(F)** Number of metabolites significantly above background in 10,000 WBM cells sorted using a 70 or 100 µm nozzle, and 0.5x or 1.0x PBS sheath fluid (n = 5 replicates per treatment in each of 3 independent experiments; the metabolites that significantly differed between 0.5x PBS versus 1x PBS sheath fluid are listed in Figure 1 – Source data 2, Supplementary Table 1). **(G)** Number of metabolites significantly above background in 10,000 sorted WBM cells or 10,000 to 100,000 pipetted WBM cells (n = 5 replicates per treatment in each of 3 independent experiments). **(H-K) H,** Principal component analysis of 10,000 sorted or pipetted HNT-34 AML (AML) cells or DND-41 T-ALL (ALL) cells (one experiment with n = 8 replicates per treatment; the metabolites that significantly differed between sorted and pipetted AML cells and between sorted and pipetted ALL cells are shown in Figure 1 – Source data 3, Supplementary Table 2 and Figure 1- Source data 4, Supplementary Table 3). Figure 1 - Source Data 8 shows the raw metabolomics data for the comparison of AML to ALL cells. **(I)** Metabolites that significantly changed between AML and ALL cells in sorted versus pipetted

samples (listed in Figure 1 – Source data 5, Supplementary Table 4). **(J, K)** Correlation between Log2 fold changes (in AML versus ALL cells) in sorted versus pipetted samples for all detected metabolites (**J**) and metabolites that significantly differed between sorted AML and ALL cells **(K**). **(L-P) L**, Number of metabolites above background in 10,000 pipetted WBM cell samples at various times after the death of the mouse (one experiment with n = 5 replicates per time point). **(M)** Number of metabolites that significantly increased or decreased at each time point relative to the 5 minute time point (the metabolites are listed in Figure 1 – Source data 6, Supplementary Table 5). **(N-P)** Log2 transformed (**N**), non-transformed (**O**), and non-transformed intensity values for metabolites < $1x10^8$ (**P**) in the 5 versus 120 minute samples. The statistical significance of differences between treatments was assessed using a paired t-test (A), a Kolmogorov–Smirnov test (B) followed by Holm-Sidak's multiple comparisons adjustment, repeated measures one-way ANOVA followed by Tukey's (D) or Dunnett's (G) multiple comparisons adjustment, repeated measures two-way ANOVA followed by Sidak's multiple comparisons adjustment (F), or Spearman correlation analysis (J, K, N-P). All statistical tests were two-sided. Data represent mean ± SD. See also Figure 1 – figure supplement 1.

Figure 2. Metabolic differences between HSC/MPPs and WBM cells.

(A) Metabolites significantly above background in 10,000 sorted HSC/MPPs or WBM cells (n = 3-7 replicates per treatment in each of 4 independent experiments; fold change > 2 and FDR < 0.05). **(B)** Metabolites that were significantly depleted (left) or enriched (right) in HSC/MPPs as compared to WBM cells (fold change > 2.5, FDR < 0.01; all metabolites with fold change > 2.0 and FDR < 0.05 are listed in Figure 2 – Source data 2, Supplementary Table 1). Data in (A) represent mean ± SD. A comparison of these differences to those observed by Agathocleous et al. (2017) between HSCs and WBM cells is shown in Figure 2 – figure supplement 1 and a summary of the differences in lipid species is shown in Figure 2 – figure supplement 2.

Figure 3. Metabolic differences between methotrexate-treated and control HSCs or circulating melanoma cells and primary tumors.

(A-D) Bone marrow cellularity **(A)** and the frequencies of $CD150^{+}CD48^{-}Lin^{-}Sca1^{+}c\text{-}kit^{+}$ HSCs (**B**), $CD150^{-}CD48^{-}Lin^{-}Sca1^{+}c\text{-}kit^{+}$ MPPs **(c)**, and $Lin^{-}Sca1^{+}c\text{-}kit^{+}$ cells **(D)** in femurs and tibias from mice treated with methotrexate or vehicle control (n = 5 mice per treatment from 2 independent experiments). **(E)** Percentage of nucleated blood cells that were donor-derived after competitive transplantation of bone marrow cells from methotrexate-treated versus control mice into irradiated recipients (two independent experiments). **(F)** AICAR levels in HSC/MPPs from mice treated with methotrexate or vehicle (11 control samples and 9 MTX samples from 4 independent experiments). **(G)** Metabolites detected above background in primary tumor cells or circulating melanoma cells (n=3 or 4 replicates per treatment in one experiment; fold change > 2 and FDR < 0.05). **(H-K)** Levels of the purines IMP **(H)**, XMP **(I)**, GMP **(J)**, and AMP **(K)** in primary tumor and circulating melanoma cells. Statistical significance was assessed by t-test (A), repeated measures two-way ANOVA (B-D) or mixed effects analysis (E) followed by Sidak's multiple comparisons adjustment. All tests were two-sided. Data represent mean ± SD. The flow cytometry gates used to isolate each cell population are shown in Figure 3 – figure supplement 1. All of the metabolites that differed between circulating melanoma cells and subcutaneous tumor cells are listed in Figure 3 – Source data 2, Supplementary Table 1.

Figure 4: Metabolomic profiling of HSCs isolated by flow cytometry. (A) Overview of the method. (**B)** Metabolites detected above background in 10,000 HSCs/MPPs in this study (green numbers, 159 metabolites total) as compared to our prior study using a different method (Agathocleous et al., 2017) (blue numbers, 57 metabolites total). These data are from one experiment, representative of 4 independent experiments. Metabolites detected above background were calculated by comparing 3 WBM or 3 HSC/MPP samples to 3 sheath fluid blanks (fold change > 2, FDR < 0.05).

SUPPLEMENTARY FIGURES

Figure 1 – figure supplement 1. Chromatographic performance of lipids separated by HILIC. (A-D) Representative chromatograms for **(A)** phosphatidylcholine (PC (36:2))**, (B**) phosphatidylethanolamine (PE (38:6)), **(C)** lysophosphatidylcholine (Lyso-PC (18:0)), and **(D)** lysophosphatidylethanolamine (Lyso-PE(20:4)). **(E-H)** Standard curves of isotopically labelled lipids from four classes of lipids we detected (black) and the corresponding endogenous lipid (red) for **(E)** phosphatidylcholine, **(F)** phosphatidylethanolamine, **(G)** lysophosphatidylcholine and **(H)** lysophosphatidylethanolamine (n = 3 replicates, data represent mean ± SD)

Figure 2 - figure supplement 1. Metabolites that were detected as differing between HSCs/MPPs and WBM cells using the Agathocleous et al. method (Agathocleous et al., 2017) versus the method described in this study. Metabolites identified by Agathocleous et al. as **(A)** enriched or **(B)** depleted in HSC/MPPs as compared to WBM cells and the results obtained for the same metabolites in the current study (data are from Figure 2).

Figure 2 - figure supplement 2. Glycerophospholipids are enriched in HSC/MPPs as compared to WBM cells. (A) Schematic of glycerophospholipid metabolism and **(B)** list of phosphatidylcholines (PC), phosphatidylethanolamines (PE), phosphatidylserines (PS), Lyso-PCs, and Lyso-PEs detected in 10,000 HSCs/MPPs or WBM cells by our method. Red metabolites were enriched in HSC/MPPs and blue metabolites were depleted in HSC/MPPs. Purple metabolites were detected but not significantly changed. Black metabolites were not detected (n = 11 replicates per cell population from a total of 4 independent experiments).

Figure 3 - figure supplement 1. Flow cytometry gating strategies. (A) Flow cytometry gating strategies for isolating $CD150^{+}CD48^{-}Lin^{-}Sca1^{+}c\text{-}kit^{+}$ HSCs (0.0057% of bone marrow cells), $CD150^{-}CD48^{-}Lin^{-}Sca1^{+}c\text{-}kit^{+}$ MPPs (0.0047% of bone marrow cells), and $Lin^{-}Sca1^{+}c\text{-}kit^{+}$ cells

(0.19% of bone marrow cells). (**B)** Flow cytometry gating strategy for isolating live $HLA^{+}DsRed^{+}mTer119^{-}mCD45^{-}mCD31^{-}$ human melanoma cells from mechanically dissociated subcutaneous tumors from xenografted NSG mice (all melanomas were tagged with stable DsRed expression). **(C)** Flow cytometry gating strategy for isolating live $HLA^{+}DsRed^{+}mTer119^{-}mCD45^{-}mCD31^{-}$ circulating melanoma cells from the blood of xenografted NSG mice.

SUPPLEMENTARY DATA

Figure 1 – Source data 1. All source data for Figure 1.

Figure 1 – Source data 2

Supplementary table 1a. Metabolites enriched or depleted in cells sorted using 1x PBS sheath fluid vs 0.5x PBS sheath fluid (fold change > 2 and FDR < 0.05). Correlation analysis of metabolite levels from 1x PBS versus 0.5x PBS samples: Spearman r = 0.995, y = 1.3x - 2142387. These metabolites were not significantly enriched in any metabolic pathway by pathway enrichment analysis.

Supplementary table 1b. Metabolites enriched or depleted in cells sorted using 1x PBS sheath fluid vs 0.5x PBS sheath fluid (fold change = 1.5 to 2 and FDR < 0.05).

Figure 1 – Source data 3

Supplementary table 2a. Metabolites enriched or depleted in sorted vs pipetted AML cells (fold change > 2 and FDR < 0.05). Correlation analysis of sorted versus pipetted AML samples: spearman r = 0.997, y = 1.1x + 214263. Metabolites that differed between sorted and pipetted AML cells were significantly enriched in “cysteine and methionine metabolism”.

Supplementary table 2b. Metabolites enriched or depleted in sorted versus pipetted AML cells (fold change = 1.5 to 2 and FDR < 0.05).

Figure 1 – Source data 4

Supplementary table 3a. Metabolites enriched or depleted in sorted vs pipetted ALL cells (fold change > 2 and FDR < 0.05). Correlation analysis: Spearman r = 0.999, y = 1.1x – 436390. The metabolites were not significantly enriched in any metabolic pathway.

Supplementary table 3b. Metabolites enriched or depleted in sorted versus pipetted ALL cells (fold change = 1.5 to 2 and FDR < 0.05).

Figure 1 – Source data 5

Supplementary table 4a – Metabolites that significantly differed between AML and ALL cells in both sorted and pipetted samples, sorted samples only, or pipetted samples only. Metabolites that significantly differed between AML and ALL cells in both sorted and pipetted samples were significantly enriched in “glycerophospholipid metabolism”. No pathways were enriched among metabolites that differed in only sorted samples or only in pipetted samples**.**

Supplementary table 4b. Metabolites that significantly differed between sorted AML and ALL cells or pipetted AML and ALL cells and for which fold change was between 1.5 and 2 in either the sorted or pipetted samples (FDR < 0.05).

Figure 1 – Source data 6

Supplementary table 5. Metabolites enriched or depleted at various time points after the incubation of cell suspensions on ice. The fold change cutoff is indicated in the left column. All are FDR < 0.05. Correlation analysis: 5 min versus 15 min: Spearman r = 0.998; 5 min versus 30 min: Spearman r = 0.996; 5 min versus 60 min: Spearman r = 0.992

Figure 1 – Source data 7

Supplementary table 6a. Metabolites enriched or depleted in WBM cells isolated from cells suspended in PBS versus HBSS (fold change > 2 and FDR > 0.05). Correlation

analysis: Spearman r = 0.960, y = 0.92x + 1759331. These metabolites were not significantly enriched in any metabolic pathway.

Supplementary table 6b. Metabolites enriched or depleted in WBM cells isolated from cells suspended in PBS versus HBSS (fold change = 1.5 to 2 and FDR < 0.05).

Figure 1 – Source data 8

The raw metabolomic analyses from experiments comparing AML and ALL cells (Figure 1H-K). These files contain the raw counts for each metabolite in each sample and the statistical comparisons between samples for each metabolite.

Figure 1 – figure supplement 1. Source data for Figure 1 – figure supplement 1.

Figure 2 – Source data 1. All source data for Figure 2.

Figure 2 – Source data 2

Supplementary table 1. Metabolites enriched or depleted in sorted HSC/MPPs as compared to WBM cells (fold change > 2 and FDR < 0.05)

Figure 3 – Source data 1. All source data for Figure 3.

Figure 3 – Source data 2

Supplementary table 1. Metabolites that differed between circulating melanoma cells and melanoma cells from primary subcutaneous tumors in xenografted mice (Fold change > 2 and P < 0.05).

Figure 4 – Source data 1. All source data for Figure 4.

Figure 1

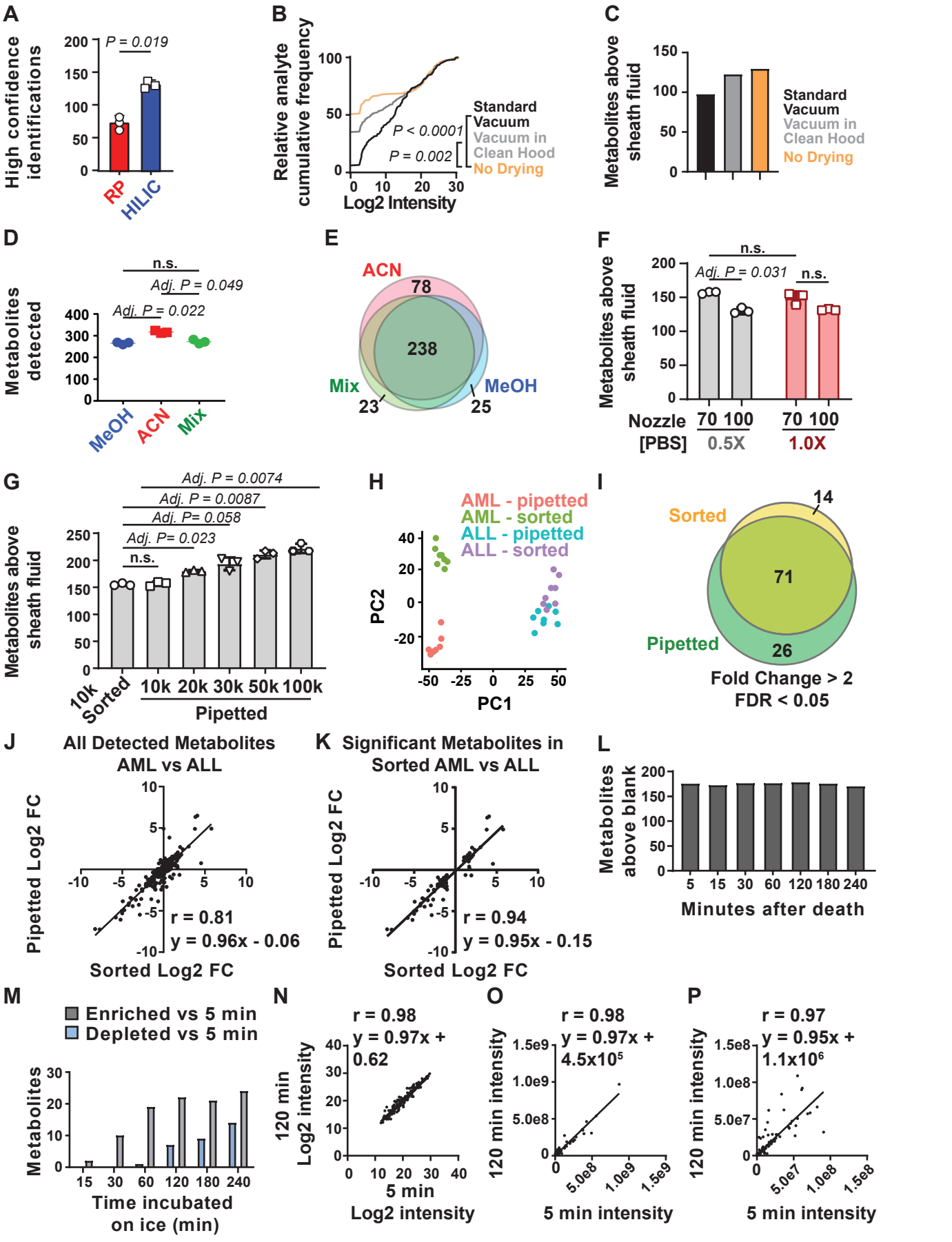
A
High confidence identifications
P = 0.019
RP
HILIC
B
Relative analyte cumulative frequency
P < 0.0001
P = 0.002
Standard Vacuum
Vacuum in Clean Hood
No Drying
Log2 Intensity
C
Metabolites above sheath fluid
Standard Vacuum
Vacuum in Clean Hood
No Drying
D
Metabolites detected
n.s.
Adj. P = 0.049
Adj. P = 0.022
MeOH
ACN
Mix
E
ACN
78
238
Mix
MeOH
23
25
F
Metabolites above sheath fluid
n.s.
Adj. P = 0.031
n.s.
Nozzle 70 100 70 100
[PBS] 0.5X 1.0X
G
Metabolites above sheath fluid
Adj. P = 0.0074
Adj. P = 0.0087
Adj. P= 0.058
Adj. P= 0.023
n.s.
10k Sorted
10k 20k 30k 50k 100k
Pipetted
H
AML - pipetted
AML - sorted
ALL - pipetted
ALL - sorted
PC2
PC1
I
Sorted
14
71
Pipetted
26
Fold Change > 2
FDR < 0.05
J
All Detected Metabolites AML vs ALL
Pipetted Log2 FC
Sorted Log2 FC
r = 0.81
y = 0.96x - 0.06
K
Significant Metabolites in Sorted AML vs ALL
Pipetted Log2 FC
Sorted Log2 FC
r = 0.94
y = 0.95x - 0.15
L
Metabolites above blank
Minutes after death
M
Enriched vs 5 min
Depleted vs 5 min
Metabolites
Time incubated on ice (min)
N
r = 0.98
y = 0.97x + 0.62
120 min Log2 intensity
5 min Log2 intensity
O
r = 0.98
y = 0.97x + 4.5x10^5
120 min intensity
5 min intensity
P
r = 0.97
y = 0.95x + 1.1x10^6
120 min intensity
5 min intensity

Figure 1 - figure supplement 1

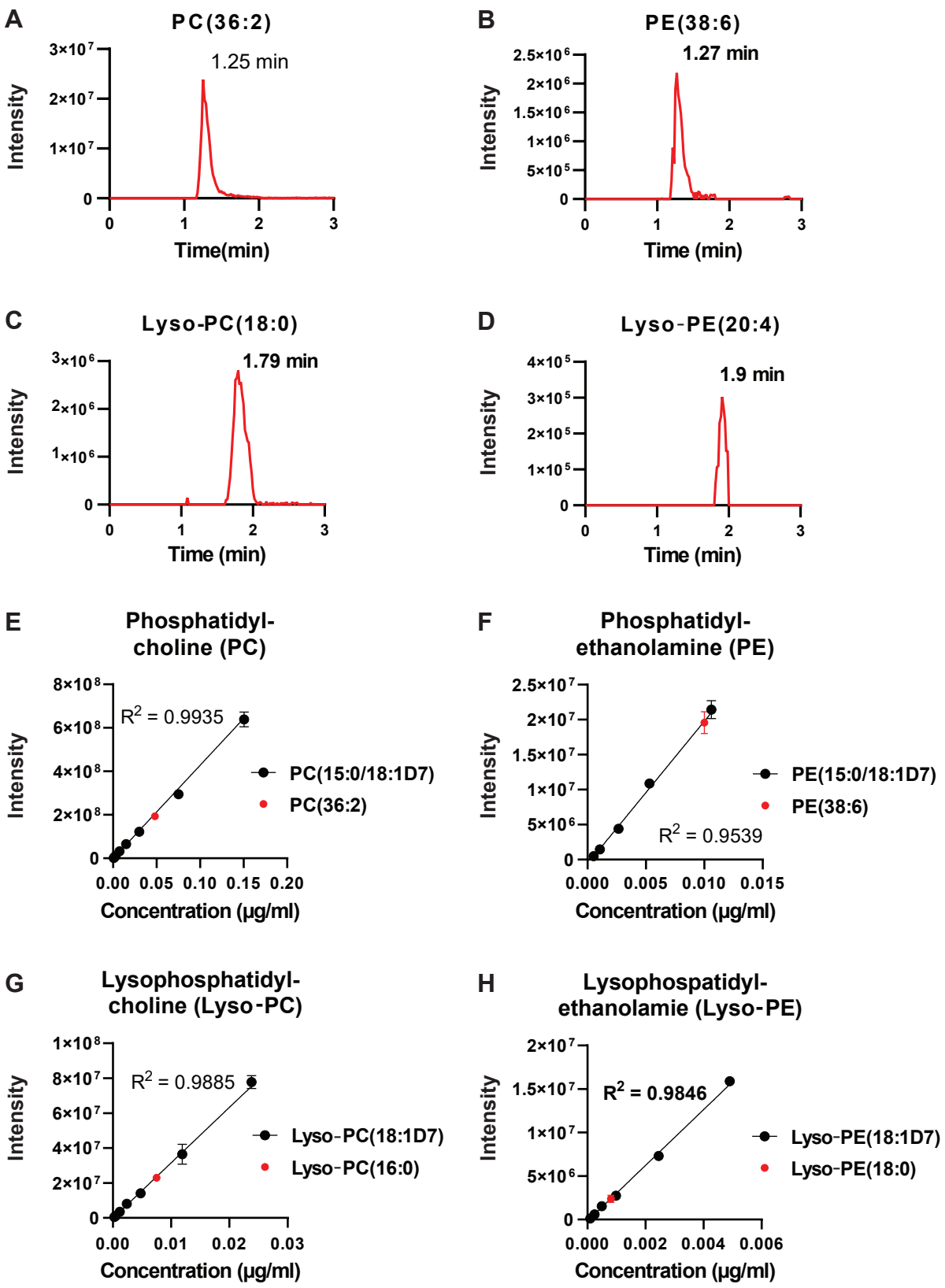

Figure 2

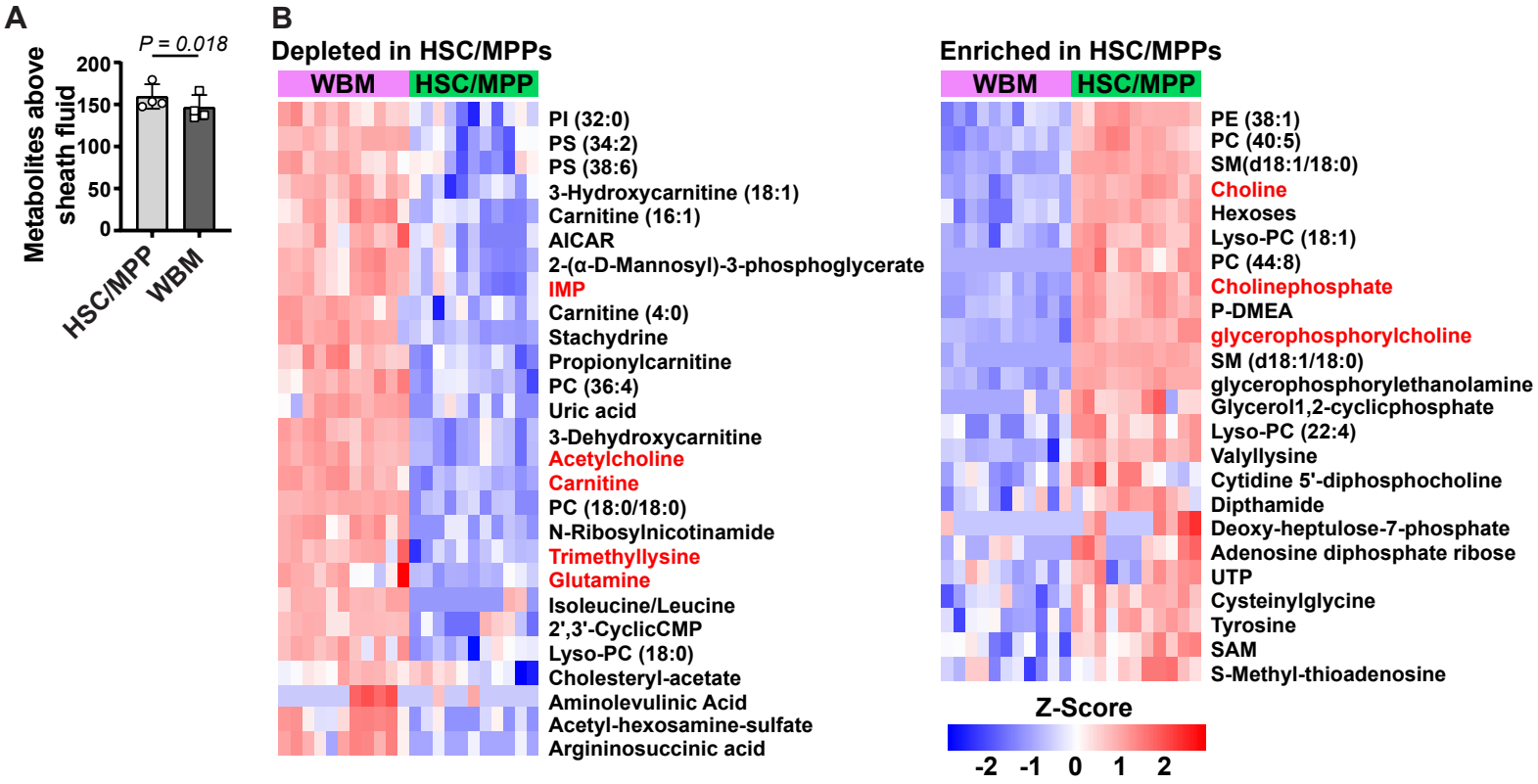
A
P = 0.018
Metabolites above sheath fluid
200
150
100
50
0
HSC/MPP
WBM
B
Depleted in HSC/MPPs
WBM
HSC/MPP
PI (32:0)
PS (34:2)
PS (38:6)
3-Hydroxycarnitine (18:1)
Carnitine (16:1)
AICAR
2-(α-D-Mannosyl)-3-phosphoglycerate
IMP
Carnitine (4:0)
Stachydrine
Propionylcarnitine
PC (36:4)
Uric acid
3-Dehydroxycarnitine
Acetylcholine
Carnitine
PC (18:0/18:0)
N-Ribosylnicotinamide
Trimethyllysine
Glutamine
Isoleucine/Leucine
2',3'-CyclicCMP
Lyso-PC (18:0)
Cholesteryl-acetate
Aminolevulinic Acid
Acetyl-hexosamine-sulfate
Argininosuccinic acid
Enriched in HSC/MPPs
WBM
HSC/MPP
PE (38:1)
PC (40:5)
SM(d18:1/18:0)
Choline
Hexoses
Lyso-PC (18:1)
PC (44:8)
Cholinephosphate
P-DMEA
glycerophosphorylcholine
SM (d18:1/18:0)
glycerophosphorylethanolamine
Glycerol1,2-cyclicphosphate
Lyso-PC (22:4)
Valyllysine
Cytidine 5'-diphosphocholine
Dipthamide
Deoxy-heptulose-7-phosphate
Adenosine diphosphate ribose
UTP
Cysteinylglycine
Tyrosine
SAM
S-Methyl-thioadenosine
Z-Score
-2 -1 0 1 2

Figure 2 - figure supplement 1

A Enriched in HSC/MPP v WBM

	Agathocleous et al		DeVilbiss et al	
Metabolite	FC	FDR	FC	FDR
glycerophosphorylcholine	34	<0.0001	29	<0.0001
ascorbate	18	0.0001	n.d. (no EDTA added)	
phosphocholine	2.7	<0.0001	4.3	<0.0001
choline	2.1	<0.0001	4.5	<0.0001
GSH	2.0	0.002	1.6	0.0025

B Depleted in HSC/MPP v WBM

	Agathocleous et al		DeVilbiss et al	
Metabolite	FC	FDR	FC	FDR
glutamine	0.18	<0.0001	0.33	<0.0001
N-acetylaspartate	0.30	<0.0001	0.57	<0.0001
hypoxanthine	0.34	<0.0001	0.46	0.048
carnitine	0.36	<0.0001	0.21	<0.0001
IMP	0.36	0.0003	0.10	<0.0001
spermidine	0.38	0.002	n.d.	
acetylcholine	0.42	<0.0001	0.37	<0.0001
trimethyllysine	0.48	<0.0001	0.27	<0.0001
betaine	0.50	<0.0001	n.d.	
glutamate	0.64	<0.0001	0.69	0.030
taurine	0.77	0.0001	0.64	<0.0001

Figure 2 - figure supplement 2

A

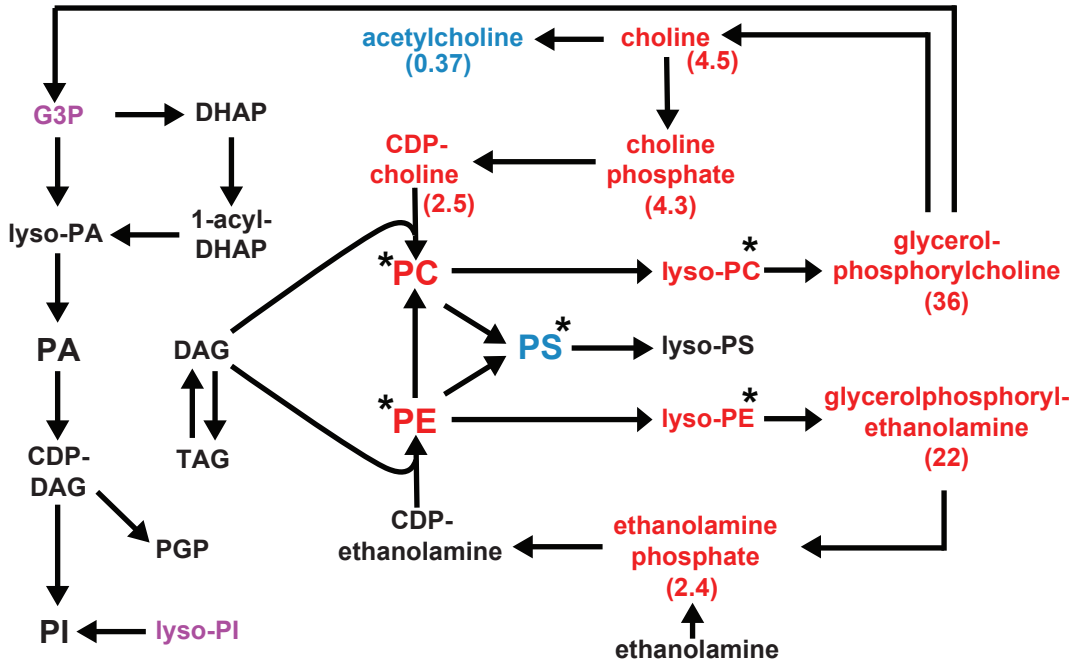

*Multiple metabolites detected in this class. See table.

Enriched in HSC/MPPs vs WBM Depleted in HSC/MPPs vs WBM Detected, No Change Not Detected

B

PC

Metabolite	FC	FDR
PC (32:0)	1.1	0.26
PC (32:1)	1.2	0.015
PC (32:2)	1.3	0.0099
PC (34:1)	2.2	0.0000
PC (34:2)	1.1	0.11
PC (36:1)	2.3	0.0000
PC (36:2)	1.3	0.0008
PC (36:4)	0.25	0.0000
PC (36:5)	1.5	0.0000
PC (38:4)	1.8	0.0000
PC (38:5)	0.37	0.024
PC (40:4)	2.4	0.0000
PC (40:5)	3.1	0.0000
PC (40:6)	1.8	0.0000
PC (40:8)	2.1	0.0000
PC (44:8)	14	0.0000

PE

Metabolite	FC	FDR
PE (32:0)	1.1	0.58
PE (34:1)	1.8	0.0000
PE (34:2)	1.1	0.22
PE (36:1)	1.7	0.0000
PE (36:2)	0.96	0.62
PE (36:3)	1.9	0.0000
PE (36:6)	0.67	0.0022
PE (38:1)	19	0.0000
PE (38:3)	1.9	0.0000
PE (38:4)	1.7	0.0000
PE (38:5)	1.8	0.0000
PE (38:6)	0.83	0.11
PE (40:5)	0.55	0.0000
PE (40:7)	0.96	0.78

PS

Metabolite	FC	FDR
PS (34:2)	0.18	0.0000
PS (36:1)	1.6	0.0000
PS (36:4)	0.99	0.90
PS (38:3)	0.83	0.037
PS (38:5)	1.3	0.0044
PS (38:6)	0.14	0.0000
PS (40:5)	0.70	0.013
PS (40:6)	0.67	0.0044
PS (40:7)	0.59	0.0064

Lyso-PC

Metabolite	FC	FDR
Lyso-PC (16:0)	1.5	0.020
Lyso-PC (18:0)	0.31	0.0013
Lyso-PC (18:1)	3.5	0.0000
Lyso-PC (18:2)	2.5	0.025
Lyso-PC (22:4)	9.7	0.0000

Lyso-PE

Metabolite	FC	FDR
Lyso-PE (16:0)	1.8	0.039
Lyso-PE (18:0)	1.4	0.013
Lyso-PE (18:1)	1.1	0.90
Lyso-PE (20:4)	1.9	0.0064

Figure 3

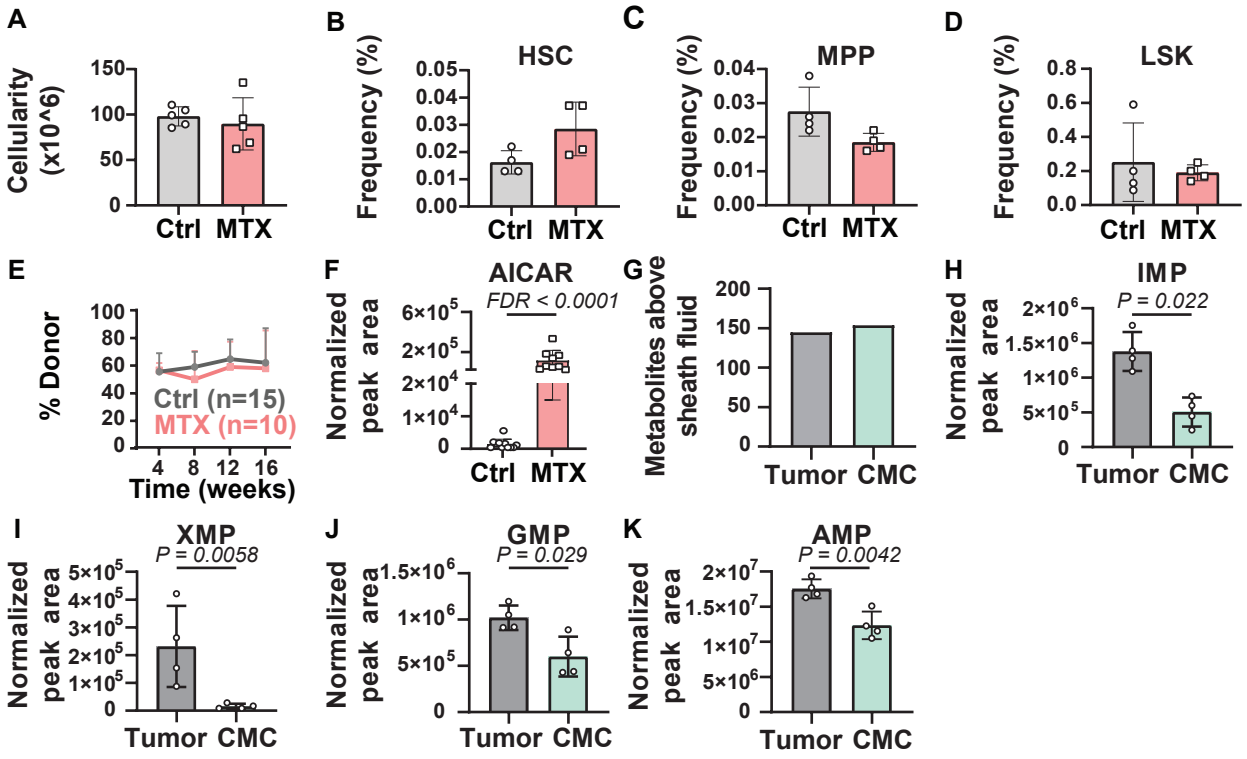
A
Cellularity (x10^6)
150
100
50
0
Ctrl MTX
B
HSC
Frequency (%)
0.05
0.04
0.03
0.02
0.01
0.00
Ctrl MTX
C
MPP
Frequency (%)
0.04
0.03
0.02
0.01
0.00
Ctrl MTX
D
LSK
Frequency (%)
0.8
0.6
0.4
0.2
0.0
Ctrl MTX
E
% Donor
100
80
60
40
20
0
Ctrl (n=15)
MTX (n=10)
4 8 12 16
Time (weeks)
F
AICAR
FDR < 0.0001
Normalized peak area
6×10^5
2×10^5
2×10^4
1×10^4
0
Ctrl MTX
G
Metabolites above sheath fluid
200
150
100
50
0
Tumor CMC
H
IMP
P = 0.022
Normalized peak area
2×10^6
1.5×10^6
1×10^6
5×10^5
0
Tumor CMC
I
XMP
P = 0.0058
Normalized peak area
5×10^5
4×10^5
3×10^5
2×10^5
1×10^5
0
Tumor CMC
J
GMP
P = 0.029
Normalized peak area
1.5×10^6
1×10^6
5×10^5
0
Tumor CMC
K
AMP
P = 0.0042
Normalized peak area
2×10^7
1.5×10^7
1×10^7
5×10^6
0
Tumor CMC

Figure 3 - figure supplement 1

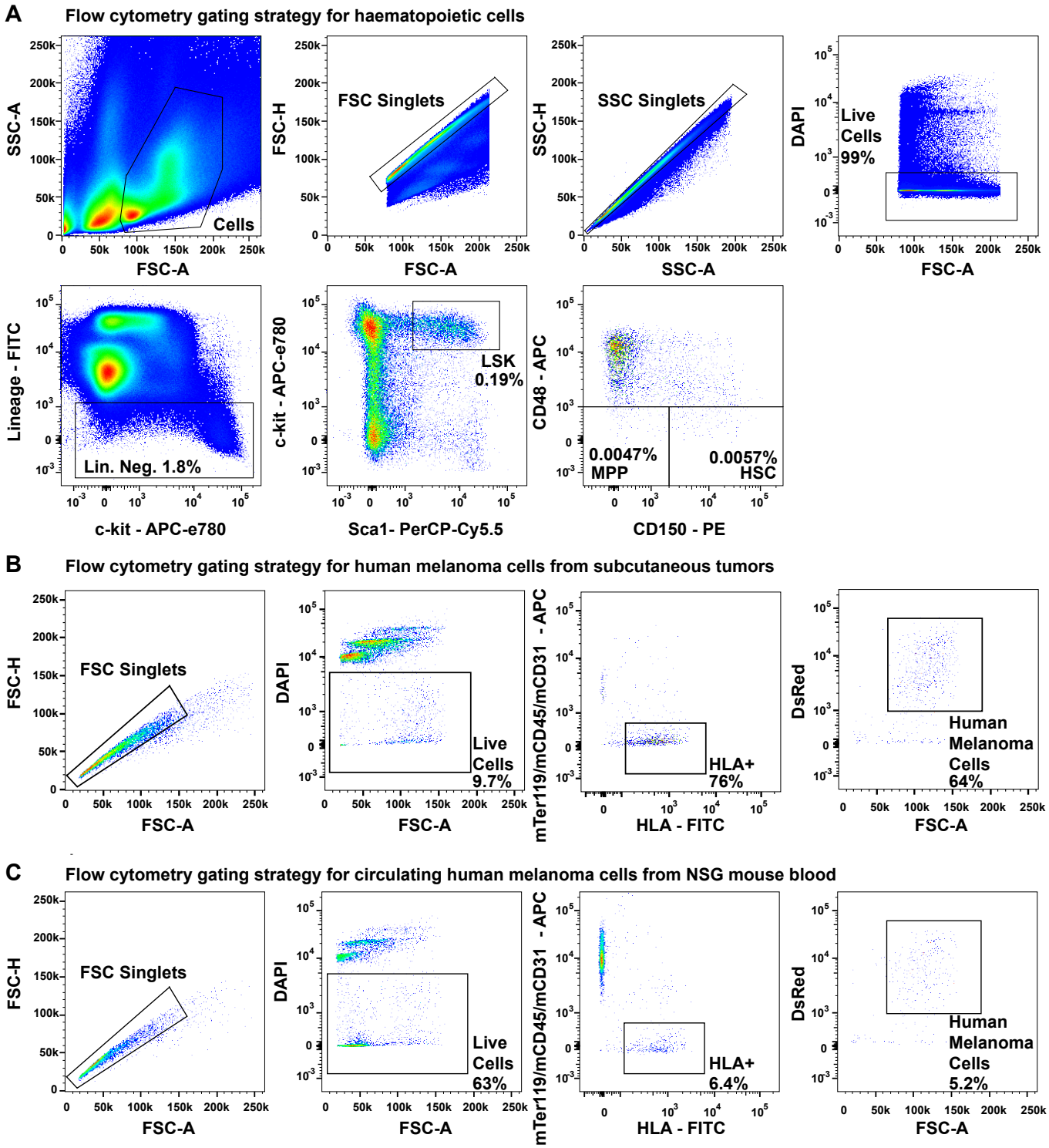

Figure 4

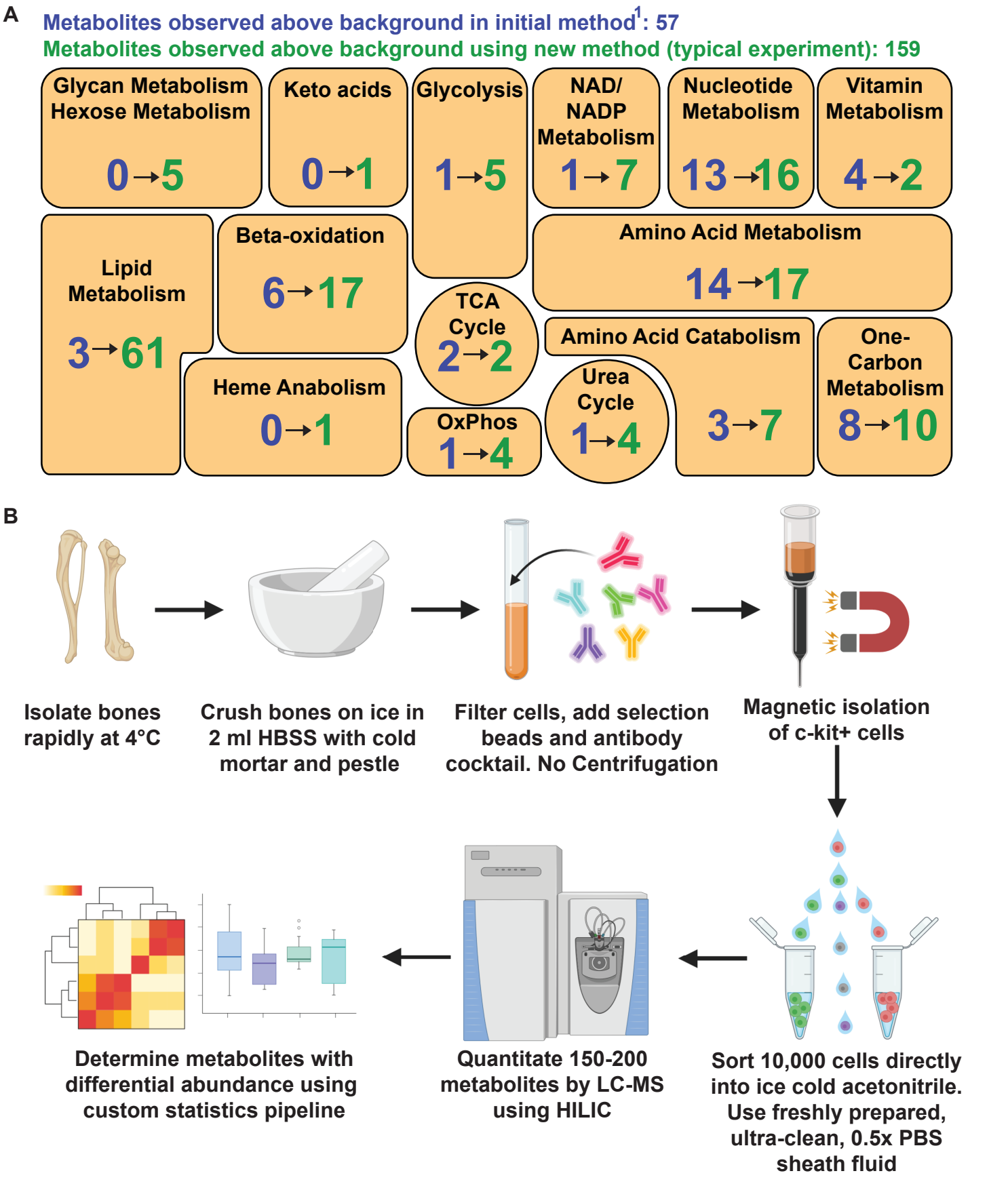
A
Metabolites observed above background in initial method[1]: 57
Metabolites observed above background using new method (typical experiment): 159
Glycan Metabolism Hexose Metabolism
0→5
Keto acids
0→1
Glycolysis
1→5
NAD/ NADP Metabolism
1→7
Nucleotide Metabolism
13→16
Vitamin Metabolism
4→2
Lipid Metabolism
3→61
Beta-oxidation
6→17
Amino Acid Metabolism
14→17
TCA Cycle
2→2
Amino Acid Catabolism
3→7
One-Carbon Metabolism
8→10
Urea Cycle
1→4
Heme Anabolism
0→1
OxPhos
1→4
B
Isolate bones rapidly at 4°C
Crush bones on ice in 2 ml HBSS with cold mortar and pestle
Filter cells, add selection beads and antibody cocktail. No Centrifugation
Magnetic isolation of c-kit+ cells
Sort 10,000 cells directly into ice cold acetonitrile. Use freshly prepared, ultra-clean, 0.5x PBS sheath fluid
Quantitate 150-200 metabolites by LC-MS using HILIC
Determine metabolites with differential abundance using custom statistics pipeline